

## R-Ras Regulates Exocytosis by Rgl2/Rlf-mediated Activation of RalA on Endosomes<sup>D V</sup>

Akiyuki Takaya,<sup>\*†</sup> Takahiro Kamio,<sup>\*</sup> Michitaka Masuda,<sup>‡</sup> Naoki Mochizuki,<sup>‡</sup> Hirofumi Sawa,<sup>§</sup> Mami Sato,<sup>§</sup> Kazuo Nagashima,<sup>§</sup> Akiko Mizutani,<sup>||</sup> Akira Matsuno,<sup>¶</sup> Etsuko Kiyokawa,<sup>†</sup> and Michiyuki Matsuda<sup>\*†</sup>

<sup>\*</sup>Department of Signal Transduction, Research Institute for Microbial Diseases, Osaka University, Yamadaoka, Osaka 565-0871, Japan; <sup>†</sup>Department of Pathology and Biology of Diseases, Graduate School of Medicine, Kyoto University, Kyoto 606-8501, Japan; <sup>‡</sup>Department of Structural Analysis, National Cardiovascular Center Research Institute, Osaka 565-8565, Japan; <sup>§</sup>Laboratory of Molecular and Cellular Pathology, Graduate School of Medicine, Hokkaido University, Sapporo 060-8638, Japan; <sup>||</sup>Basic Medical Science and Molecular Medicine, Tokai University School of Medicine, Kanagawa 259-1193, Japan; and <sup>¶</sup>Department of Neurosurgery, Teikyo University Ichihara Hospital, Chiba 299-0111, Japan

Submitted August 29, 2006; Revised February 16, 2007; Accepted February 28, 2007  
Monitoring Editor: Mark Ginsberg

R-Ras is a Ras-family small GTPase that regulates various cellular functions such as apoptosis and cell adhesion. Here, we demonstrate a role of R-Ras in exocytosis. By the use of specific anti-R-Ras antibody, we found that R-Ras was enriched on both early and recycling endosomes in a wide range of cell lines. Using a fluorescence resonance energy transfer-based probe for R-Ras activity, R-Ras activity was found to be higher on endosomes than on the plasma membrane. This high R-Ras activity on the endosomes correlated with the accumulation of an R-Ras effector, the Rgl2/Rlf guanine nucleotide exchange factor for RalA, and also with high RalA activity. The essential role played by R-Ras in inducing high levels of RalA activity on the endosomes was evidenced by the short hairpin RNA (shRNA)-mediated suppression of R-Ras and by the expression of R-Ras GAP. In agreement with the reported role of RalA in exocytosis, the shRNA of either R-Ras or RalA was found to suppress calcium-triggered exocytosis in PC12 pheochromocytoma cells. These data revealed that R-Ras activates RalA on endosomes and that it thereby positively regulates exocytosis.

### INTRODUCTION

R-Ras is a Ras-family GTPase and its amino acid sequence is 55% identical to those of the classical types of Ras (H-, K-, N-Ras, collectively referred to hereafter as “Ras”) (Lowe *et al.*, 1987). As is the case with the other Ras-family GTPases, R-Ras is regulated primarily by two classes of protein, guanine nucleotide exchange factor (GEF) and GTPase-activating protein (GAP). Reflecting the high sequence similarity among Ras-family GTPases, many GEFs and GAPs for R-Ras catalyze other Ras-family GTPases as well (Ohba *et al.*, 2000). Furthermore, R-Ras is known to interact with many effectors of Ras, such as Raf-1, Ral GEFs, and the p110 $\alpha$  subunit of phosphoinositide 3-kinase (PI3K) (Rey *et al.*, 1994; Spaargaren and Bischoff, 1994; Spaargaren *et al.*, 1994; Marte *et al.*, 1997). Despite this redundancy between R-Ras and Ras, R-Ras

exhibits various properties that are distinct from those of Ras. For example, R-Ras preferentially activates Ral GEFs and PI3K, but it does not activate Raf (Huff *et al.*, 1997; Rodriguez-Viciana *et al.*, 2004). The transforming activity of constitutively active R-Ras is substantially less potent than that of the constitutively active Ras (Cox *et al.*, 1994), although it should be noted that a recent report has suggested the involvement of R-Ras in human gastric cancer (Nishigaki *et al.*, 2005). Meanwhile, R-Ras is known to regulate cell adhesion, cell spreading, and phagocytosis through the activation of integrin (Zhang *et al.*, 1996; Keely *et al.*, 1999; Berrier *et al.*, 2000; Self *et al.*, 2001). R-Ras-null mice have recently been shown to exhibit excessive vascular responses, in spite of the fact that they are otherwise normal (Komatsu and Ruoslahti, 2005). This phenotype seems to reflect higher levels of expression of R-Ras in smooth muscle cells, including blood vessel cells. The results obtained with R-Ras-null mice have also demonstrated that an R-Ras defect can be almost entirely compensated for by other gene products.

Ral GEFs, effectors of Ras-family GTPases, are activators of the two Ral proteins, RalA and RalB, which are also Ras-family GTPases (Wolthuis and Bos, 1999; Quilliam *et al.*, 2002; Rodriguez-Viciana *et al.*, 2004). It has been suggested that this Ral GEFs-Ral pathway is more important in the Ras-dependent oncogenesis of human cells than are other Ras-dependent pathways, such as those involving Raf and PI3K (Hamad *et al.*, 2002; Rangarajan *et al.*, 2004; Lim *et al.*, 2005; Gonzalez-Garcia *et al.*, 2005). The activated Ral then binds to various Ral-binding proteins and thereby regulates

This article was published online ahead of print in *MBC in Press* (<http://www.molbiolcell.org/cgi/doi/10.1091/mbc.E06-08-0765>) on March 7, 2007.

<sup>D V</sup> The online version of this article contains supplemental material at *MBC Online* (<http://www.molbiolcell.org>).

Address correspondence to: Michiyuki Matsuda ([matsudam@path1.kyoto-u.ac.jp](mailto:matsudam@path1.kyoto-u.ac.jp)).

Abbreviations used: EGF, epidermal growth factor; FRET, fluorescence (Förster's) resonance energy transfer; GAP, GTPase-activating protein; GEF, guanine nucleotide exchange factor; NPY, neuropeptide Y; PI3K, p110 $\alpha$  subunit of phosphoinositide-3-kinase.

various cellular functions (Feig, 2003). The characterization of such Ral effector proteins has suggested that Ral may be involved in vesicular trafficking. For example, the Ral-binding protein RalBP1 is thought to regulate endocytosis, suggesting the involvement of Ral in endocytosis (Nakashima *et al.*, 1999). Ral may also regulate exocytosis, because Ral binds to two components of the exocyst complex, Sec5 and Exo84 (Moskalenko *et al.*, 2002, 2003).

The exocyst complex was originally identified by genetic and biochemical studies as a cluster of molecules required for exocytosis in budding yeast, and it was later characterized in a wide range of eukaryotes. The exocyst complex consists of eight subunits: Sec3, Sec5, Sec6, Sec8, Sec10, Sec15, Exo70, and Exo84 (Lipschutz and Mostov, 2002). These proteins are primarily involved in the tethering and/or docking process of trafficking vesicles, which occurs before the fusion process (Finger *et al.*, 1998; Tsuboi *et al.*, 2005). Due to their fundamental role in exocytosis, any malfunction of the proteins in the exocyst complex can disrupt various cellular events, such as the basolateral transport of vesicles in polarized epithelial cells, neurite outgrowth in PC12 cells, paraxial mesoderm formation in mice, and secretory vesicle-mediated abscission in *Drosophila* (Friedrich *et al.*, 1997; Grindstaff *et al.*, 1998; Vega and Hsu, 2001; Murthy *et al.*, 2003; Gromley *et al.*, 2005).

To gain a better understanding of the function of R-Ras and its potential role in Ral-mediated exocytosis, it will be essential to elucidate not only the subcellular localization but also the activity change of these proteins. Thus, we developed specific anti-R-Ras sera and a probe for R-Ras activity based on the principle of fluorescence resonance energy transfer (FRET), a technique that has been shown to be extremely useful for the spatiotemporal analysis of small GTPases (Kurokawa *et al.*, 2004b). Using these tools, we found that endogenous R-Ras is enriched and activated at endosomes and that these R-Ras proteins promote exocytosis by activating RalA.

## MATERIALS AND METHODS

### Probes Based on FRET

FRET probes for R-Ras, designated as Raichu-R-Ras, were prepared essentially as described previously (Mochizuki *et al.*, 2001; Takaya *et al.*, 2004). From the amino terminus, Raichu-R-Ras consisted of a modified yellow fluorescent protein (YFP) designated as "Venus" (Nagai *et al.*, 2002) (amino acids [aa] 1-239), a spacer (Leu-Asp), human R-Ras (aa 1-199), a 17-amino acid-spacer (Gly-Gly-Thr-Gly-Gly-Gly-Gly-Gly-Ser-Gly-Thr-Gly-Gly-Gly-Thr), the Ras-binding domain of RalGDS (aa 785-871), a spacer (Gly-Gly-Arg), a modified cyan fluorescent protein (CFP) designated as "SECFP" (Lys<sup>27</sup>Arg, Asp<sup>130</sup>Ala, Asn<sup>165</sup>His, Ser<sup>176</sup>Gly) (aa 1-237), a spacer (Gly-Arg-Ser-Arg), and the carboxy-terminal region of R-Ras (aa 195-218) (Figure 1A). The characterization of Raichu R-Ras was performed as described previously (Takaya *et al.*, 2004).

### Plasmids

pCXN2-mCFP, pCXN2-mRFP, and pCXN2-mCherry are expression vectors encoding a monomeric SECFP (Zacharias *et al.*, 2002), a monomeric red fluorescent protein (RFP) (Kurokawa *et al.*, 2004a), and mCherry, respectively. cDNA of mCherry was provided by R. Y. Tsien (University of California at San Diego). The pRedNLS and pRedMito expression vectors contain an internal ribosomal site followed by the cDNAs of DsRed-Express (Clontech, Mountain View, CA) with nuclear and mitochondrial localization signals, respectively (Aoki *et al.*, 2005). pCXN2-5Myc and pCXN2-Flag are mammalian expression vectors containing Myc and Flag epitope tags, respectively. cDNAs of RalBP1 and Rgl were provided by A. Kikuchi (Hiroshima University, Hiroshima, Japan). cDNA of p110 $\alpha$  and p85 $\alpha$  were obtained from Y. Fukui (University of Tokyo, Tokyo, Japan), and cDNA of Rab5A was obtained from Y. Takai (Osaka University, Osaka, Japan). Rap1B cDNA was provided by N. Minato (Kyoto University, Kyoto, Japan). The cDNAs of K-Ras and N-Ras were obtained from L. A. Feig (Tufts University, Boston, MA). cDNAs of Rab7, Rab11A, and RalB were purchased from Guthrie cDNA Resource Center (Sayre, PA). pAcGFP1-Endo was purchased from Clontech. pVenus-

N1-NPY was obtained from A. Miyawaki (The Brain Science Institute, RIKEN, Wako-shi, Japan) (Nagai *et al.*, 2002). pHA-EYFP-GH1 has been described previously (Matsuno *et al.*, 2005). pCXN2-Flag-CalDAG-GEFII, pCXN2-Flag-CalDAG-GEFIII, pCXN2-Flag-R-RasGAP, pCAGGS-Flag-p120RasGAP, pCXN2-Flag-rap1GAP1B, pCAGGS-RasGRF, pCAGGS-mSos1, and pEF-BOS-myc-Gap1<sup>tm</sup> have been described previously (Yamamoto *et al.*, 1995; Gotoh *et al.*, 1997; Ohba *et al.*, 2000). pCXN2-5Myc-R-Ras-rRNAi (RNA interference-resistant clone) encodes a R-Ras mutant resistant to the short hairpin RNA (shRNA) vector. For the preparation of the glutathione S-transferase (GST) fusion proteins, cDNAs were subcloned into pGEX vectors and recombinant proteins were prepared according to the manufacturer's protocol (GE Healthcare, Little Chalfont, Buckinghamshire, United Kingdom).

### Cells, Antibodies, and Reagents

293T cells were obtained from B. J. Mayer (University of Connecticut, Storrs, CT). The line of Cos7 cells used in this study was Cos7/E3, a subclone of Cos7 cells established by Y. Fukui. The PC12 cells were obtained from S. Kuroda (University of Tokyo). HeLa and Madin-Darby canine kidney (MDCK) cells were purchased from the Human Science Research Resources Bank (Sennan-shi, Osaka, Japan). The GH3 cells used here have been described previously (Matsuno *et al.*, 2005). The PC12 cells were maintained in DMEM (Sigma-Aldrich, St. Louis, MO) supplemented with 10% fetal calf serum and 5% horse serum. GH3 cells were cultured in Ham's F-10 (Sigma-Aldrich) supplemented with 15% horse serum and 2.5% fetal calf serum. Other cells were maintained in DMEM supplemented with 10% fetal calf serum. GH3 cells stably expressing R-Ras were prepared essentially as described previously (Akagi *et al.*, 2003). Anti-green fluorescent protein (GFP) rabbit serum was prepared in our laboratory. Anti-RalA and anti-RalB were purchased from BD Biosciences (San Jose, CA). Anti-FLAG M2 and tetradecanoyl phorbol-13-acetate (TPA) was purchased from Sigma-Aldrich. Anti-Myc 9E10 was obtained from Santa Cruz Biotechnology (Santa Cruz, CA). Anti-GFP antibody was also purchased from Takara Bio (Otsu, Japan). Anti-Akt, anti-phospho Akt (Thr308), anti-phospho-mitogen-activated protein kinase kinase (MEK) 1/2 (Ser217/221), and anti-R-Ras were purchased from Cell Signaling Technology (Beverly, MA). Alexa 488 anti-rabbit immunoglobulin G (IgG), Alexa 488 anti-rat IgG, and Alexa 568 anti-mouse IgG were purchased from Invitrogen (San Diego, CA). To generate anti-R-Ras sera, three rabbits were injected with GST-R-Ras.

### RNA Interference

Synthetic siRNAs against R-Ras and Ral proteins were prepared as described previously (Oinuma *et al.*, 2004; Wozniak *et al.*, 2005). siRNAs were transfected using Oligofectamine or Lipofectamine 2000 (Invitrogen) according to the manufacturer's instructions. pSuper-retro-puro vector (OligoEngine, Seattle, WA) was used for short hairpin RNA. The shRNA sequences for rat R-Ras and RalA have been described previously (Oinuma *et al.*, 2004; Vitale *et al.*, 2005), and the sequence for rat RalB was 5'-GCCGACAGTTACAGAAAGA-3'. After transfection, the cells were incubated for at least 48 h before analysis.

### Bos' Pull-Down Assay

Bos' pull-down assay for Ral proteins was performed essentially as described previously (Takaya *et al.*, 2004). Briefly, the cells were lysed in Ral buffer (50 mM Tris-HCl, pH 7.5, 200 mM NaCl, 2.5 mM MgCl<sub>2</sub>, 1% NP-40, 10% glycerol, 1 mM Na<sub>3</sub>VO<sub>4</sub>, 1 mM phenylmethylsulfonyl fluoride, 10  $\mu$ g/ml aprotinin, and 10  $\mu$ g/ml leupeptin) and were clarified by centrifugation. The supernatant was incubated with GST-Sec5-RBD or GST-RalBP1-RBD for 30 min at 4°C. The resulting complexes of Ral-GTP and GST fusion proteins were incubated with glutathione-Sepharose beads (GE Healthcare) for 1 h at 4°C, and after the bound proteins and cell lysates had been separated by SDS-polyacrylamide gel electrophoresis (PAGE), immunoblotting with anti-RalA or anti-RalB antibody was carried out. Bound antibodies were detected by an ECL chemiluminescence detection system (GE Healthcare), and binding was quantified with the aid of an LAS-1000 image analyzer (Fuji-Film, Tokyo, Japan). The pull-down assay for Ras, Rap1, and R-Ras was performed essentially as described above except for the use of GST-RalGDS-RBD.

### Immunoprecipitation

Transfected Cos7 cells were harvested in ice-cold lysis buffer (50 mM Tris-HCl, pH 7.5, 200 mM NaCl, 2.5 mM MgCl<sub>2</sub>, 1% NP-40, 0.5% sodium deoxycholate, 10% glycerol, 1 mM Na<sub>3</sub>VO<sub>4</sub>, 1 mM phenylmethylsulfonyl fluoride, 10  $\mu$ g/ml aprotinin, and 10  $\mu$ g/ml leupeptin). Anti-Myc antibody, GFP antiserum, or R-Ras antiserum was added to the cleared lysates. After the lysates were subjected to 1 h of rotation at 4°C with protein G-Sepharose or protein A-Sepharose (GE Healthcare), the beads were washed and boiled in sample buffer. The bound proteins were then subjected to immunoblot analysis.

### Immunohistochemistry and Immunogold Electron Microscopy

Formalin-fixed, paraffin-embedded sections were deparaffinized with xylenes and rehydrated with ethanol. The sections were treated with normal goat serum and 1% H<sub>2</sub>O<sub>2</sub> to quench endogenous peroxidase activity, and then they

were incubated with primary antibody overnight at 4°C. After incubation of the sections with the biotinylated secondary antibody, immunopositive signals were visualized using 3,3'-diaminobenzidine tetrahydrochloride as a chromogen. For immunogold electron microscopy, the cells were fixed with 4% paraformaldehyde, 0.35% glutaraldehyde, and 0.2% picric acid at 4°C for 1.5 h, followed by fixation with 4% paraformaldehyde and 0.2% picric acid overnight at 4°C. After being washed with phosphate-buffered saline (PBS), the cells were dehydrated with ethanol and embedded in Lowicryl K4M (Polysciences; Tokyo, Japan). Ultrathin sections were placed on nickel grids and were immersed in a target retrieval solution (Dako Denmark, Glostrup, Denmark). Then, the samples were exposed to microwave radiation for 20 min, after which they were washed with distilled water. The grids were incubated with anti-R-Ras or preimmune rabbit serum at room temperature for 2 h, and then they were incubated for 1 h with anti-rabbit IgG labeled with 10-nm gold particles (GE Healthcare). After being washed and dried, the sections were stained with both uranyl acetate and lead citrate; the sections were then examined with a Hitachi H-800 transmission electron microscope (Hitachi High-Technologies, Tokyo, Japan). In some experiments, MDCK cells expressing an endosomal marker protein, AcGFP-Endo, were used for the analysis. Cells were double stained with anti-R-Ras rabbit serum and anti-GFP mouse monoclonal antibody (mAb) JL-8, which were detected with anti-rabbit IgG labeled with 5-nm gold particles and anti-mouse IgG labeled with 10-nm gold particles, respectively. As a control, anti-R-Ras rabbit serum preadsorbed to GST-R-Ras, preimmune rabbit serum, nonspecific rabbit IgG, or nonspecific mouse IgG was also used.

### Immunocytochemistry

To stain the endogenous R-Ras protein, MDCK cells were fixed with 3.7% formaldehyde and then subjected to refixation with methanol at -20°C and permeabilization with 0.2% Triton X-100, followed by incubation in PBS containing 3% bovine serum albumin (BSA) and 0.02% Triton X-100 for 1 h. In some experiments, MDCK cells were fixed with 4% paraformaldehyde, immediately followed by permeabilization with 0.01% Triton X-100 for 1 min and incubation with 2% BSA in 50 mM NH<sub>4</sub>Cl-containing PBS. These fixed cells were incubated for 1 h at room temperature with anti R-Ras rabbit serum, washed with PBS, and then incubated for 30 min at room temperature with Alexa 488 anti-rabbit IgG. For the 3HA-tag and 5Myc-tag staining, Cos7 cells were fixed with 3% paraformaldehyde and subjected to permeabilization and staining as described above. Alexa 488 anti-rat IgG and Alexa 568 anti-mouse IgG were used to detect anti-hemagglutinin (HA) and anti-Myc, respectively. After being washed, the cells were imaged with an FV-500 confocal microscope equipped with an argon laser and with an HeNe laser microscope (Olympus, Tokyo, Japan). Twenty-five XY images scanned from the bottom to the top of the cells were obtained to prepare stacked images of XY and XZ sections.

### Imaging of R-Ras and Ra1A Activity in Living Cells

R-Ras and Ra1A activity was visualized with Raichu-R-Ras or Raichu-Ra1A essentially as described previously (Mochizuki *et al.*, 2001; Takaya *et al.*, 2004). Expression plasmids were transfected into Cos7 cells by Polyfect (QIAGEN, Valencia, CA) or 293fectin (Invitrogen). More than 36 h after transfection, the cells were imaged with an Olympus IX70 inverted microscope equipped with an image splitter, Dual-View (Optical Insights, Santa Fe, NM) and an EMCCD camera, iXon DV887 (Andor Technology, Belfast, United Kingdom), and the imaging process was controlled by MetaMorph software (Molecular Devices, Sunnyvale, CA). In some experiments, cells were imaged with an Olympus IX81 inverted microscope equipped with a laser-based autofocusing system, IX2-ZDC, and an automatically programmable XY stage, MD-XY30100T-Meta, which allowed us to obtain the time-lapse images of several view fields in a single experiment. For dual-emission ratio imaging of the Raichu probes, we used previously described filter sets (Takaya *et al.*, 2004), and we obtained images for CFP and FRET. After background subtraction was carried out, the FRET/CFP ratio was depicted using MetaMorph software, and this image was used to represent FRET efficiency. Confocal FRET images were obtained by an IX51 upright fluorescence microscope (Olympus) equipped with a CSU-10 spinning Nipkow disk confocal unit (Yokogawa, Tokyo, Japan), a W-view (Hamamatsu Photonics, Hamamatsu, Japan), and a diode-pumped solid state 430-nm laser (Melles Griot, Carlsbad, CA).

### Exocytosis Assay

The exocytosis assay was carried out using Venus-tagged neuropeptide Y (NPY) as described previously (Nagai *et al.*, 2002). pVenus-N1-NPY or pHA-EYFP-GH1 with or without additional expression vectors was transfected into PC12 cells or GH3 cells with Lipofectamine 2000 (Invitrogen). Sixty hours after transfection, the cells were washed in a low-potassium saline solution (145 mM NaCl, 5.6 mM KCl, 2.2 mM CaCl<sub>2</sub>, 0.5 mM MgCl<sub>2</sub>, 5.6 mM glucose, and 15 mM HEPES, pH 7.4). Then, the medium was exchanged for a high-potassium saline medium (95 mM NaCl, 56 mM KCl, 2.2 mM CaCl<sub>2</sub>, 0.5 mM MgCl<sub>2</sub>, 5.6 mM glucose, and 15 mM HEPES, pH 7.4) to depolarize the cells. After 20 min in the case of the PC12 cells or 10 min in the case of the GH3 cells, cell-free supernatants were collected and were stored as the secreted fraction. Cells remaining on the culture dishes were lysed in PBS containing 1% Triton

X-100, and they were cleared by centrifugation to obtain the nonsecreted fraction. The fluorescence of NPY-Venus or EYFP-GH1 recovered in each fraction was measured by a FluoroSkan II fluorescence microplate reader (Global Medical Instrumentation, Ramsey, MN).

### Online Supplemental Material

Time-lapse FRET images of Supplemental Figure S3J and Figure 3B are compiled into QuickTime videos available as supplemental material. Movie 1 shows Cos7 cells transfected with pRaichu-R-Ras and stimulated with TPA as described in the legend to Supplemental Figure S3K. Movie 2 shows Cos7 cells transfected with pRaichu-R-Ras as described in the legend to Figure 2B. Images were acquired every 30 s, and the video is displayed at 15 frames per second. Supplemental Figures 1–6 show characterization of anti-R-Ras serum, images of colocalization studies, basic property of Raichu-R-Ras probe, and results of coimmunoprecipitation studies.

## RESULTS

### Tissue Distribution of Endogenous R-Ras

One of the reasons why the biological function of R-Ras remains elusive may be the lack of information concerning its tissue distribution and subcellular localization, which in turn is likely due to the lack of a specific antiserum. Therefore, we developed high-affinity anti-R-Ras sera that could be used for immunohistochemistry. One of the antisera was found to specifically recognize the endogenous R-Ras protein by immunoblotting analysis (Supplemental Figure S1). The obtained anti-R-Ras serum was used for immunohistochemical analyses. We found that R-Ras accumulated at high levels in the cytoplasm of smooth muscle cells, including those in the intestine and blood vessels, as has been reported recently (Komatsu and Ruoslahti, 2005) (Figure 1A). To a lesser extent, R-Ras expression was also observed in the neuroendocrine cells of the adrenal medulla and in islet cells in the pancreas (Figure 1B). Immunohistochemistry analysis in other tissues is described in Supplemental Figure S2.

### Localization of Endogenous R-Ras on the Vesicular Structures Related to Early and Recycling Endosomes

To more closely analyze the subcellular distribution of R-Ras, we chose MDCK cells, which were found to express R-Ras most abundantly among the cell lines examined (Supplemental Figure S1C). Quantitative immunoblotting analysis revealed that the number of R-Ras molecules was  $1.5 \times 10^5$ /cell, which was about one fifth of the number of Ras molecules but similar to the numbers of Ra1A and Ra1B molecules (data not shown). In MDCK cells, endogenous R-Ras was enriched on the vesicles and/or on endosome-like structures, although weak staining of the plasma membrane was also clearly seen (Figure 1, C and D). Such vesicular structures were not observed with preimmune sera or anti-R-Ras serum preadsorbed with antigen (data not shown). To further investigate the nature of R-Ras-positive endosomes, R-Ras was coexpressed with endosomal markers (Figure 2). R-Ras localization was found to overlap significantly with that of transferrin (early and recycling endosomes), Rab4A (early and recycling endosomes), Rab5A (early endosome), and Rab11A (recycling endosome), but not with that of EEA1 (early endosome) and Rab7 (late endosome). Immunoelectron micrographs showed that R-Ras was localized on cytoplasmic vesicular structures that were ~50 nm in diameter (Figure 1E). Furthermore, double staining showed the colocalization of R-Ras and AcGFP-Endo, an endosomal marker (Figure 1F). These results indicated that the R-Ras-loaded vesicles were related to early and recycling endosomes, but not to the late endosomes.

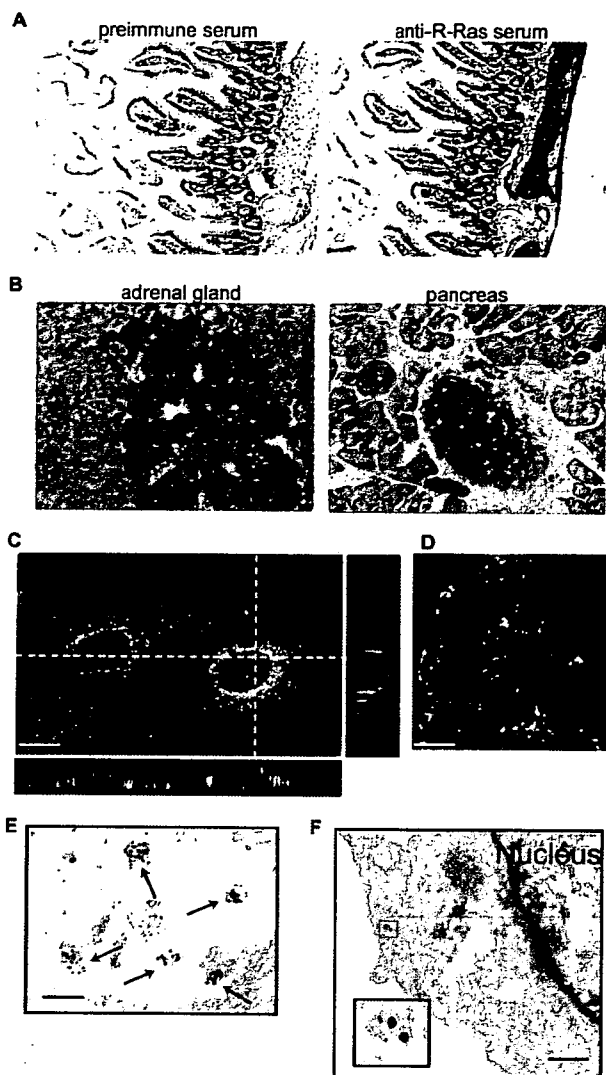


**Figure 1.** Tissue distribution and subcellular localization of R-Ras. (A) Immunohistochemistry analysis of mouse intestine with preimmune (left) or anti-R-Ras serum (right). Bound antibodies were detected with diaminobenzidine tetrahydrochloride, and the nuclei were counterstained with hematoxylin. Note the staining of the smooth muscle cell layer. (B) Immunohistochemistry of the mouse adrenal gland and pancreas. Note the staining of the adrenal medulla and Langerhans' islands. MDCK cells were fixed in 3.7% formaldehyde and methanol (C) or 4% paraformaldehyde (D) as described in the text, stained with the anti-R-Ras serum and the Alexa 488-coupled anti-rabbit IgG antibody, and observed with a confocal fluorescent microscope. Twenty-five XY images were obtained from the bottom to the top of the cells to prepare the stacked XY image. Cross sections are also shown at the dotted lines. Bar, 10  $\mu$ m. (E) Immunoelectron micrograph of a MDCK cell stained with anti-R-Ras serum before detection with anti-rabbit IgG labeled with 10-nm gold particles. Bar, 100 nm. (F) Immunoelectron micrograph of a MDCK cell expressing an endosomal marker protein, AcGFP-Endo. Cells were double-stained with anti-R-Ras rabbit serum and anti-GFP mouse mAb JL-8, which were detected with anti-rabbit IgG labeled with 5-nm gold particles and anti-mouse IgG labeled with 10-nm gold particles, respectively. Inset depicts the magnified image of the gold particles. Bar, 100 nm.

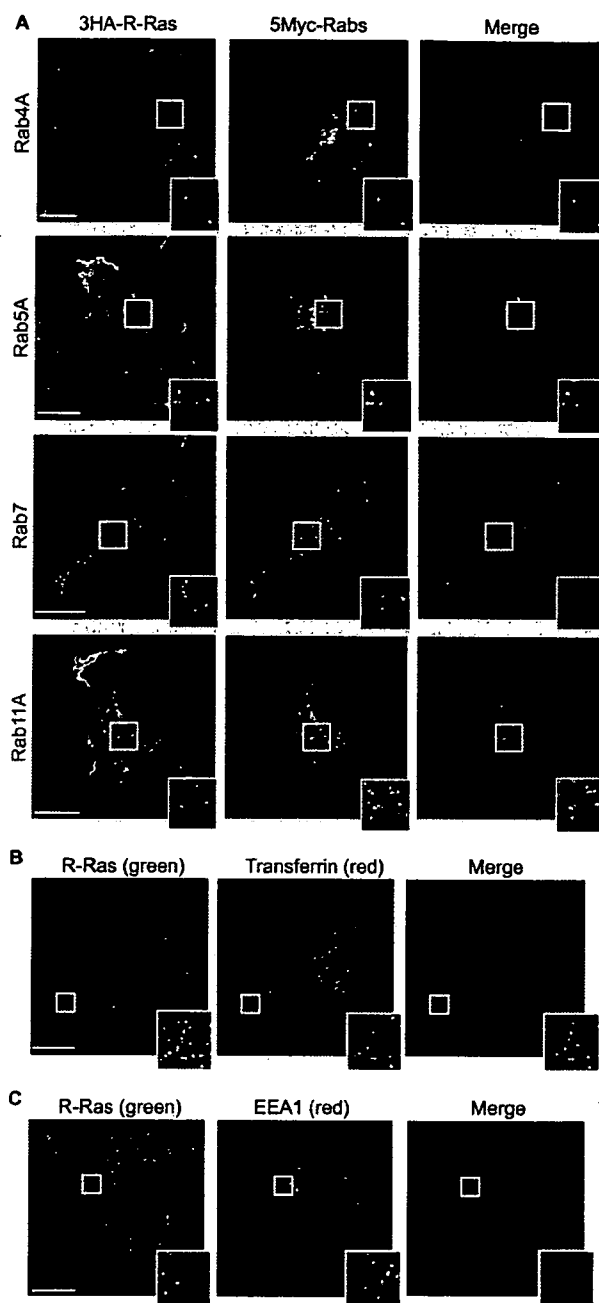


**Figure 2.** Colocalization of R-Ras with early and recycling endosome markers. (A) Cos7 cells expressing 3HA-tagged R-Ras and 5Myc-tagged Rab4A (early and recycling endosome marker), Rab5A (early endosome marker), Rab7 (late endosome marker), or Rab11A (recycling endosome marker) were double stained with anti-HA and anti-Myc antibodies and then observed with a laser-scanning confocal microscope. In the merged images, the red and green areas indicate anti-Myc and anti-HA antibodies, respectively. Bar, 10  $\mu$ m. Outlined regions were enlarged and are shown in the insets. (B) Cos7 cells were incubated with Alexa-568-conjugated transferrin for 60 min and then stained with anti-R-Ras serum. (C) Cos7 cells were double stained with anti-R-Ras serum and anti-EEA1 antibody. Bar, 10  $\mu$ m. Outlined regions were enlarged and are shown in the insets.

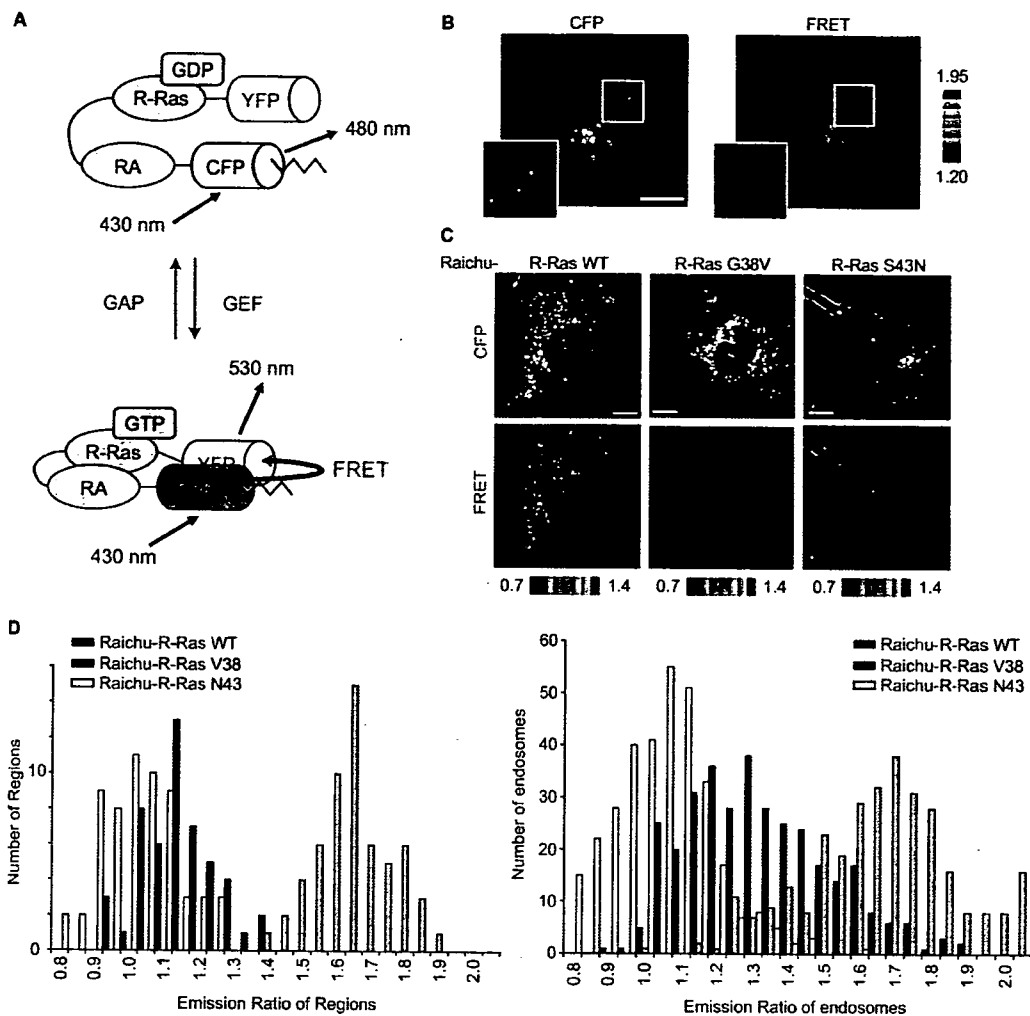


**Figure 3.** High R-Ras activity on the endosomes. (A) Schematic representation of the Raichu-R-Ras probe. Raichu-R-Ras consisted of a modified YFP designated as Venus, R-Ras, the RA domain (RA) of RalGDS, a modified CFP designated as SECFP, and the carboxy-terminal hypervariable region of R-Ras (indicated by the zigzag lines). On R-Ras activation, the intramolecular binding of R-Ras to the RA domain brings CFP into proximity with YFP, evoking YFP-derived fluorescence by the sensitized FRET. (B) A Cos7 cell expressing Raichu-R-Ras was imaged for CFP (excitation 430 nm/emission 480 nm) and YFP (excitation 430 nm/emission 530 nm). The images of the ratio (YFP versus CFP) were generated to represent the level of FRET. The upper and lower limits of the ratio range are shown on the right. Outlined regions are shown enlarged in the insets. Bar, 10  $\mu$ m. (C) Cos7 cells expressing Raichu-R-Ras and its mutants were imaged with a confocal microscope. Bar, 10  $\mu$ m. (D) FRET efficiency (YFP/CFP ratio) of Raichu-R-Ras, Raichu-R-Ras G38V, and Raichu-R-Ras S43N at the plasma membrane (left) and on the endosomes (right). For the endosomes, regions that exhibited higher CFP intensity than an appropriate threshold level were selected, and their YFP and CFP intensities were obtained. For the plasma membrane, three appropriate regions were arbitrarily selected, and their YFP and CFP intensities were obtained. Data from at least seven cells are shown in the histograms.

#### Development of a Probe for R-Ras, Raichu-R-Ras

The unexpected observation that R-Ras was enriched on the endosomes urged us to investigate the role played by R-Ras on endosomes. For this purpose, we developed a series of FRET probes for the live-cell imaging of R-Ras activity. For the sake of brevity, only the results obtained with the Raichu-205X probe (hereafter referred to as "Raichu-R-Ras") are described here, because this probe performed best among those tested. From the amino terminus, Raichu-R-Ras includes a modified YFP designated as Venus, human R-Ras (aa 1-199), the Ras-association domain of RalGDS (aa 785-871), a modified CFP referred to as SECFP, and the carboxy-terminal hypervariable region of R-Ras (aa 195-218) (Figure

3A). Raichu-R-Ras fulfills most requirements for a FRET probe as described in the Supplemental Material and Supplemental Figure S3.

#### Activation of R-Ras on Endosomes

Using Raichu-R-Ras, we visualized R-Ras activity in living Cos7 cells. The distribution of the Raichu-R-Ras probe was indistinguishable from that of the authentic R-Ras: The probe was enriched on the endosomes, but also localized diffusely on the plasma membrane (Figure 3B, Supplemental Figure S4, and Supplemental Movie 2). R-Ras activity, as visualized by the FRET level, was higher on the endosomes than on the plasma membrane. The high R-Ras activity observed on endosomes was more clearly observed with a

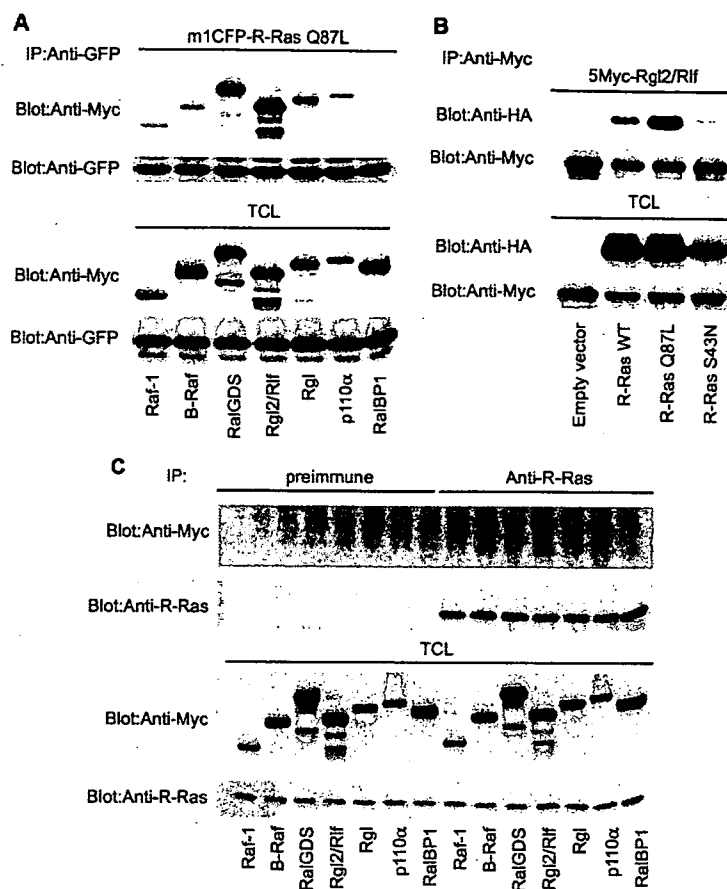


**Figure 4.** Binding of R-Ras to Rgl2/Rlf. (A) Cos7 cells expressing m1CFP-tagged R-Ras-Q87L and the Myc-tagged effector proteins indicated at the bottom of the panel were used for the analysis. In p110 $\alpha$  expression, p85 $\alpha$  was used for coexpression to stabilize the PI3K heterodimer complex. From the cell lysates, GFP-tagged proteins were immunoprecipitated, and bound proteins were analyzed by immunoblotting with anti-Myc mAb or anti-GFP mAb. (B) Cos7 cells expressing HA-tagged R-Ras mutants and Myc-tagged Rgl2/Rlf were lysed and analyzed as described in A. (C) Endogenous R-Ras protein was immunoprecipitated with anti-R-Ras serum from Cos7 cells expressing the Myc-tagged effector proteins. The immunoprecipitates were analyzed as described in A. Preimmune serum was used as a control.

spinning disk confocal unit (Figure 3C). To exclude the possibility that the high FRET level on the endosomes was caused by accumulation of the probe, we used control probes, i.e., Raichu-R-Ras G38V and Raichu-R-Ras S43N, the properties of which are shown in Supplemental Figure S3. The FRET level was diffusely high on both the plasma membrane and on endosomes in cells expressing Raichu-R-Ras G38V (Figure 3, C and D). In contrast, cells expressing Raichu-R-Ras S43N showed low levels of FRET, both on the plasma membrane and on endosomes (Figure 3, C and D). The intensity of the probe on each endosome did not affect the emission ratio of sensitized FRET over CFP in either the Raichu-R-Ras wild type, G38V mutant, or S43N mutant (data not shown). Therefore, these results negated the possibility that the high FRET signal observed on the endosomes of Raichu-R-Ras-expressing cells was caused by an accumulation of the probe. Interestingly, we could not observe remarkable difference in the localization of the wild-type and mutant Raichu-Ras proteins. This is probably because the effector domain of R-Ras-GTP is masked by the Ras-binding domain of the probe and suggests that the localization of the probe was determined primarily by the carboxy terminus of R-Ras.

#### Endosomal Localization of Rgl2/Rlf, an R-Ras Effector

Next, we attempted to identify the signaling molecules downstream of R-Ras on the endosomes. To this end, we first compared the affinity of R-Ras for Raf-1, B-Raf, RalGDS, Rgl2/Rlf, Rgl, and the p110 $\alpha$  subunit of PI3K, all of which

are known to bind to a wide range of Ras-family GTPases (Figure 4A). K-Ras and Rap1A were used as controls for the GTPases (Supplemental Figure S5A). In a coimmunoprecipitation assay, a constitutively active mutant of R-Ras (R-Ras Q87L) was found to interact most strongly with three GEFs for Ral, i.e., RalGDS, Rgl, and Rgl2/Rlf, and less strongly with Raf-1, B-Raf, and p110 $\alpha$ . These interactions were shown to depend on GTP loading, because the R-Ras Q87L mutant showed a markedly higher affinity for Rgl2/Rlf than did the wild-type protein and the nucleotide-free mutant, R-Ras S43N (Figure 4B). However, it should be noted that the high-affinity binding detected by coimmunoprecipitation does not necessarily indicate the signaling strength between the two associated proteins. Thus, we examined the effect of the activated R-Ras mutant, R-Ras Q87L, on the activity of downstream effectors. In agreement with the coimmunoprecipitation experiments, RalA, RalB, and Akt1 (downstream of p110 PI3K), but not MEK1 (downstream of the Raf proteins), were activated by R-Ras Q87L (Supplemental Figure S5). Next, we used R-Ras antiserum to examine whether the endogenous R-Ras protein is also associated with Ras effectors. Among the effector proteins tested, Rgl2/Rlf exhibited the strongest affinity for endogenous R-Ras (Figure 4C). Finally, we confirmed that Rgl2/Rlf, but not Raf-1 or p110 $\alpha$ , colocalized efficiently with R-Ras on the endosomes (Figure 5, A and B). This endosomal colocalization of Rgl2/Rlf with R-Ras was abrogated by the expression of R-RasGAP (Figure 5C). These results strongly suggested that R-Ras is bound to Rgl2/Rlf on endosomes in a GTP-dependent manner.

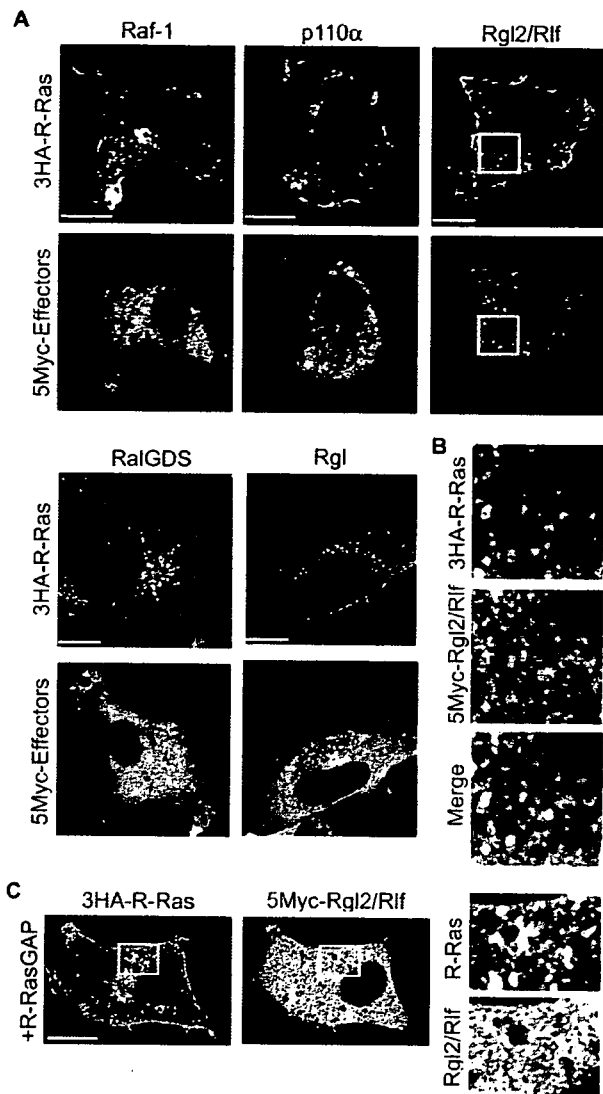


**Figure 5.** Colocalization of R-Ras with Rgl2/Rlf. (A) Cos7 cells expressing HA-tagged R-Ras and Myc-tagged R-Ras effector proteins were stained with anti-HA and Myc-tagged R-Ras effector proteins were stained with anti-HA and anti-Myc antibodies, and the cells were observed by confocal microscopy. Bar, 10  $\mu$ m. (B) Enlarged images of the outlined regions in A. In the merged image, green and red indicate 3HA-R-Ras and 5Myc-Rgl2/Rlf, respectively. (C) Cos7 cells expressing HA-tagged R-Ras, Myc-tagged Rgl2/Rlf, and R-RasGAP were stained with anti-HA and anti-Myc antibodies. Right panels are enlarged images of the outlined regions in the left panels.

#### Regulation of Vesicular RalA Activity by R-Ras

We next addressed the question of whether R-Ras regulates the activities of Ral proteins on the endosomes. In results that were consistent with those of a previous report (Shipitsin and Feig, 2004), RalA and RalB were detected both on the plasma membrane and on endosomes (Supplemental Figure S4C). Because colocalization with R-Ras was clearer in the case of RalA than RalB, we focused on RalA and examined the RalA activity on endosomes by use of Raichu-RalA, a marker for RalA activity (Takaya *et al.*, 2004) (Figure 6). In contrast to the FRET images obtained with Raichu-R-Ras, the FRET level varied significantly among endosomes, sug-

gesting that RalA activity varied among different types of endosomes (Figure 6A). We considered it likely that such differences in RalA activity among endosomes might have depended on the presence of active R-Ras; therefore, we examined RalA activity in cells expressing R-RasGAP or shRNA for R-Ras. Under both conditions, the number of endosomes showing high RalA activity was reduced significantly (Figure 6, B–D). This shRNA-mediated decrease in RalA activity was recovered by the coexpression of exogenous R-Ras, the cDNA of which harbors mutations in the shRNA-binding sequence. The dependence of RalA activity on R-Ras was confirmed by a pull-down assay with the RalA-binding region of RalBP1; the net amount of GTP-RalA was thus shown to have decreased by 20% (Figure 6E). It should be noted that the basal GTP level of RalA is  $\sim$ 7% of total guanine nucleotides bound to RalA (Takaya *et al.*, 2004). Therefore, if we assume based on the immunofluorescence data that the proportion of RalA on the endosomes is significantly smaller than that at the plasma membrane, a 20% decrease in the net amount of GTP-RalA seemed to be consistent with the significant reduction in the number of endosomes showing a high GTP-RalA level, as demonstrated by Raichu-RalA. Finally, we found that knockdown of Rgl2/Rlf profoundly decreased the RalA activity on the endosomes, suggesting that the R-Ras–Rgl2/Rlf complex is the principal activator of RalA on the endosomes (Figure 6F).

#### Requirement of R-Ras and RalA for Calcium-dependent Exocytosis

It has been reported that RalA is engaged in calcium-triggered exocytosis (Moskalenko *et al.*, 2002; Vitale *et al.*, 2005), which prompted us to examine the role played by R-Ras in the same process. YFP-tagged NPY and rat growth hormone (rGH) were used as markers of exocytosis (Nagai *et al.*, 2002; Matsuno *et al.*, 2005) (Figure 7 and Supplemental Figure S4C). In PC12 cells, depolarization-induced NPY secretion was as significantly inhibited by the expression of active R-Ras (Q87L) and R-RasGAP as by the expression of active RalA (G23V) and Rab11a (Q70L). The expression levels of recombinant proteins were examined by a quantitative immunoblotting analysis (Supplemental Figure S6). Because the expression of Rab11a T22N was less than R-Ras or RalA mutants, the ineffectiveness of this particular mutant might be ascribable to its low expression level. The role played by R-Ras and RalA was further confirmed with small interfering RNA (siRNA) (Figure 7B). The reduction of R-Ras and RalA inhibited depolarization-induced NPY secretion to a similar extent. Among the three Ral GEFs knocked down by siRNA, only the reduction of Rgl2/Rlf had an inhibitory effect on NPY secretion (Figure 7C). In GH3 pituitary adenoma cells, in which the level of expression of endogenous R-Ras was found to be low, the exogenous expression of R-Ras significantly enhanced the depolarization-induced exocytosis of both rGH and NPY (Figure 7D). The enhancement by R-Ras was abrogated by the knockdown of either R-Ras or RalA (Figure 7E). These results demonstrated that R-Ras is involved in depolarization-induced exocytosis, most likely due to the activation of Ral proteins. Furthermore, the finding that not only inhibition but also constitutive activation of R-Ras inhibits exocytosis suggests that the on-off cycle of R-Ras is required for this process.

#### DISCUSSION

We propose the following scenario for the role of R-Ras on endosomes: 1) R-Ras is activated on the surface of recycling and early endosomes, and it remains active on the vesicles

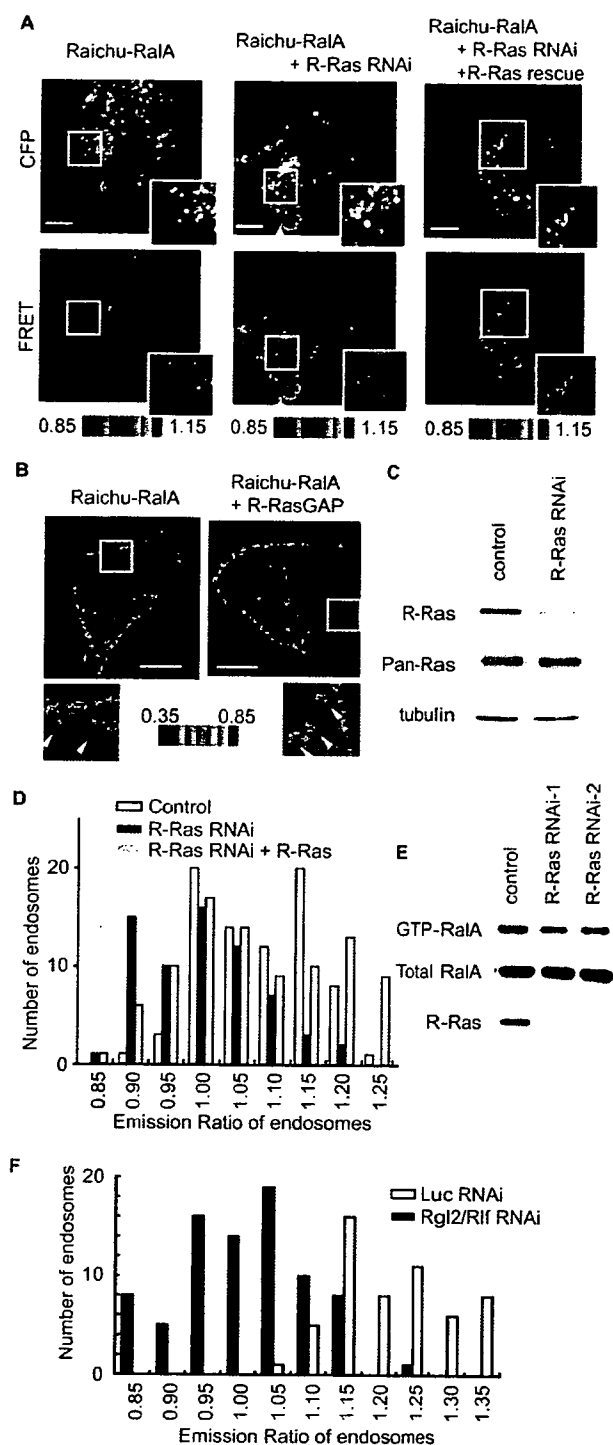


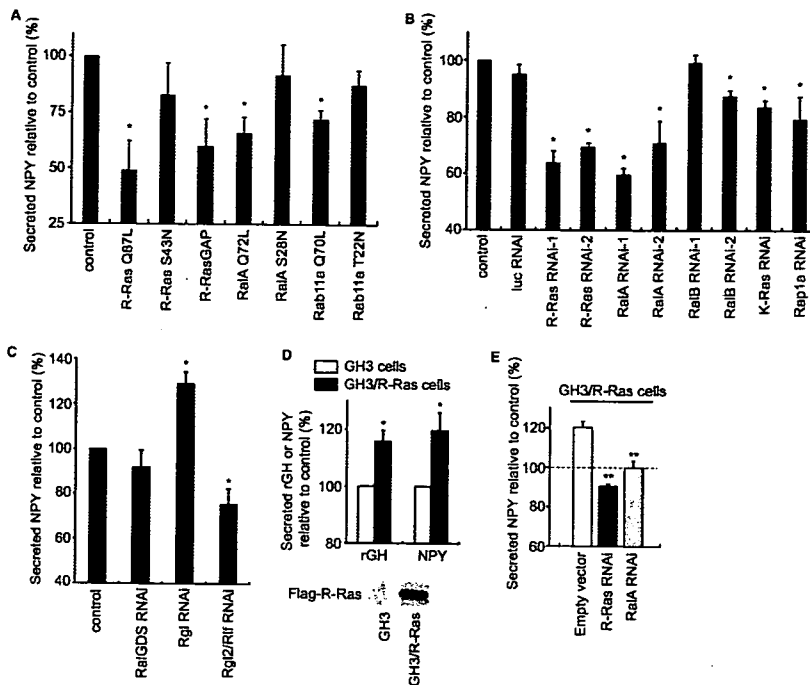
**Figure 6.** Effect of R-Ras knockdown on RalA activity on the endosomes. (A) Cos7 cells were transfected with expression vectors as indicated at the top of the panel. For knockdown, we used pSuper-R-Ras, an shRNA vector. For the rescue from knockdown, an R-Ras mutant resistant to the shRNA vector was expressed. Sixty hours after transfection, CFP and FRET images were obtained with a spinning confocal microscope. (B) MDCK cells were transfected with expression vectors as indicated at the top of the panel and imaged 20 h after transfection as in A. Outlined regions were enlarged and are shown in the insets. Arrowheads indicate representative vesicles. Bar, 10  $\mu$ m. (C) Cells transfected with an empty

derived from these endosomes. 2) The active R-Ras on these vesicles recruits Ral GEF(s). Among the candidate proteins, Rgl2/Rlf is the most plausible, because R-Ras activates both Rgl and Rgl2/Rlf more efficiently than it does RalGDS (Rodriguez-Viciana *et al.*, 2004), and also because the endogenous R-Ras was found to colocalize with Rgl2/Rlf (Figure 5). However, other Ral GEFs that are also known to bind to R-Ras (Nancy *et al.*, 1999; Shao and Andres, 2000; Rodriguez-Viciana *et al.*, 2004) may be recruited to R-Ras on endosomes in other cell types. 3) These R-Ras-recruited Ral GEFs on the endosomes activate RalA, followed by the recruitment of RalA effectors to the endosomes. Among these effectors is Exo84, a component of the exocyst complex, which marks a microdomain at the plasma membrane as a delivery site for exocytotic vesicles (Grindstaff *et al.*, 1998; Yeaman *et al.*, 2001; Inoue *et al.*, 2003). 4) The R-Ras-loaded vesicles from endosomes are tethered to the plasma membrane via the exocyst complex. It has been demonstrated that the interaction between RalA and the exocyst complex is essential for exocytosis (Moskalenko *et al.*, 2002; Polzin *et al.*, 2002; Shipitsin and Feig, 2004), and the inhibition of the exocyst complex has been shown to impair calcium-triggered exocytosis (Tsuboi *et al.*, 2005). Therefore, our observations that R-Ras was required for the calcium-induced secretion of NPY and rGH (Figure 7) are suggestive of the positive role played by R-Ras in the formation of the exocyst complex.

Another prediction contained in our model, but not directly assessed, is that RalA regulates the assembly of the exocyst complex, both on the vesicles and on the plasma membrane, by means of binding to different components of the exocyst complex: RalA interacts not only with Exo84 but also with Sec5, another component of the exocyst complex (Feig, 2003). Sec5 is primarily present on the plasma membrane, whereas Exo84 is localized primarily on the vesicles (Moskalenko *et al.*, 2003). In this context, it should be noted that RalA is activated on the plasma membrane either by Ras-dependent or by calcium-dependent pathways (Hofer *et al.*, 1998; Wolhuis and Bos, 1999). Hence, the tethering of vesicles may be promoted by the two portions of the exocyst complex, both of which are anchored to the lipid membranes via RalA. One portion consists of subunits containing Exo84 and is anchored to the endosomes and/or the vesicles and endosomes by R-Ras-activated RalA, whereas the other portion consists of subunits containing Sec5, and it is anchored to the plasma membrane by either Ras or calcium. The results have thus far suggested that the high activity of R-Ras and RalA on the surface of vesicles is constitutive rather than stimulation regulated. Therefore, RalA activity at the plasma membrane, but not that on

pSuper vector and pSuper-R-Ras were selected as described in A, and the proteins were analyzed by immunoblotting with the antibodies shown on the left. (D) Histogram of the FRET level of Raichu-RalA on the endosomes. The histograms were drawn from the data obtained from 79 endosomes in four Cos7 cells, those obtained from 66 endosomes in six pSuper-R-Ras-expressing Cos7 cells and those obtained from 89 endosomes in nine Cos7 cells expressing both pSuper-R-Ras and pCXN2-5Myc-R-Ras-rRNAi. (E) HeLa cells were transfected with control siRNA or two different siRNAs for R-Ras. After 72 h, GTP-RalA levels in the cells were analyzed by Bos' pull-down method with GST-RalBP1-RBD. The knockdown of R-Ras was also confirmed by immunoblotting. (F) The histograms were drawn from the data obtained from 55 endosomes in two Raichu-RalA-expressing Cos7 cells transfected with siRNA for luciferase and those obtained from 83 endosomes in three Raichu-RalA-expressing Cos7 cells transfected with siRNA for Rgl2/Rlf.





RalA. Depolarization-induced secretion of NPY was examined as described in A. The symbols indicate the results of *t* test analysis; \*\**p* < 0.001 compared with the control (GH3/R-Ras cells).

endosomes, may play a regulatory role in the assembly of the complete exocyst complex. In agreement with this view, we have shown that RalA is locally activated in the nascent lamellipodia of epidermal growth factor (EGF)-stimulated or migrating cells (Takaya *et al.*, 2004). Because exocytosis plays critical roles in EGF-induced membrane ruffling and cell migration (Bretscher and Aguado-Velasco, 1998; Schmoranzler *et al.*, 2003; Proux-Gillardeaux *et al.*, 2005; Tayeb *et al.*, 2005), RalA activation at the site of the membrane protrusion may indicate its role in the transport of lipid bilayer and/or integral proteins via exocytosis.

In agreement with the results of a previous report showing that RalA but not RalB regulates the delivery of E-cadherin in MDCK cells (Shipitsin and Feig, 2004), we found that only RalA was involved in calcium-triggered exocytosis (Figure 7). This difference between the two Ral proteins with respect to their involvement in exocytosis may be ascribable not only to the low binding affinity of RalB to Sec5 (Shipitsin and Feig, 2004) but also to the predominant localization of RalB on the plasma membrane (Shipitsin and Feig, 2004; Lim *et al.*, 2005).

Currently, the mechanism underlying the high R-Ras activity on the endosomes remains unknown. A dominant-negative mutant of R-Ras has been shown to be more enriched on endosomes than is the wild-type protein (Furuhjelm and Peranen, 2003). Because a dominant-negative mutant of Ras family GTPases sequesters GEFs (Feig, 1999), these observations strongly suggest that the GEFs for R-Ras are enriched on endosomes. In contrast to RalA on the vesicles, the activity of R-Ras on the vesicles seems constant (Figures 3C and 6A). Thus, R-Ras may be activated as soon as nascent R-Ras is recruited to the vesicles and inactivated when the vesicles are fused to the plasma membrane. Although none of the GEFs for R-Ras (i.e., RasGRF1, CalDAG-GEF-I/RasGRP2, CalDAG-GEF-II/RasGRP1, CalDAG-GEF-III/RasGRP3, and C3G) have been shown to localize on the endosomes (Ohba

*et al.*, 2000), this failure to detect GEFs on the endosomes may simply reflect a lack of high-affinity antibodies that could be applied for immunostaining. Interestingly, GAPs for R-Ras seem to localize primarily on the plasma membrane (Anderson *et al.*, 1990; Margolis *et al.*, 1990; Cozier *et al.*, 2003; Oinuma *et al.*, 2004). Thus, R-Ras would be expected to be inactivated when it is transported from the endosomes to the plasma membrane. This inactivation of R-Ras might serve to liberate the components of the exocyst complex and send them back into the cytoplasm or to send R-Ras back to the endosomes from the plasma membrane.

Previous studies have implicated R-Ras in the activation of integrin (Zhang *et al.*, 1996; Keely *et al.*, 1999; Berrier *et al.*, 2000; Self *et al.*, 2001; Oinuma *et al.*, 2006) and also in cell migration and adhesion (Nakada *et al.*, 2005; Wozniak *et al.*, 2005); however, the molecular mechanisms underlying these phenomena remain elusive. Our finding that the R-Ras-Rgl2/Rlf-RalA pathway regulates exocytosis may account for some of these biological activities of R-Ras. It is already known that the inhibition of exocytosis impairs integrin recycling and thereby also cell migration and cell adhesion (Proux-Gillardeaux *et al.*, 2005; Tayeb *et al.*, 2005). Hence, the inhibition of integrin by the suppression of R-Ras might initially be caused by the disruption of exocytosis. Although no direct evidence supporting the involvement of RalA in the recycling of integrin has yet been reported, Ral proteins have been shown to be implicated in cell migration (Gildea *et al.*, 2002; Takaya *et al.*, 2004; Oxford *et al.*, 2005), a process in which integrin is thought to be coordinately activated and inactivated. Therefore, it is reasonable to speculate that the R-Ras-Rgl2/Rlf-RalA pathway is involved in the recycling of integrin and thereby also in the regulation of integrin activity.

In conclusion, we observed high R-Ras activity on early and recycling endosomes. This high R-Ras activity recruits Rlf/Rgl2 and thereby activates RalA, followed by the assembly of a portion of the exocyst complex. Importantly, in

addition to RalA, other low-molecular-weight GTPases belonging to different families (i.e., TC10, Arf6, and Rab11) are also known to interact with the exocyst complex (Prigent *et al.*, 2003; Inoue *et al.*, 2003; Zhang *et al.*, 2004; Wu *et al.*, 2005). Further study will be needed to determine whether these GTPases of different families coordinately regulate the exocyst complex on the same endosomes, or whether there are distinct classes of endosomes containing only some of these GTPases. It would be of particular importance to examine the dynamic activity changes of these GTPases during the vesicular transport, which would be best examined by FRET-based imaging techniques used here.

## ACKNOWLEDGMENTS

We thank L. A. Feig, R. Y. Tsieng, Y. Fukui, K. Kaibuchi, A. Kikuchi, S. Kuroda, B. J. Mayer, N. Minato, A. Miyawaki, and Y. Takai for the provision of reagents and N. Yoshida, N. Fujimoto, and K. Fukuhara for technical assistance. This work was supported by grants-in-aid for scientific research and for cancer research from the Ministry of Education, Science, Sports and Culture of Japan, and by a grant from the Health Science Foundation of Japan. A.T. was supported by Research Fellowships from the Japan Society for the Promotion of Science for Young Scientists.

## REFERENCES

- Akagi, T., Sasai, K., and Hanafusa, H. (2003). Refractory nature of normal human diploid fibroblasts with respect to oncogene-mediated transformation. *Proc. Natl. Acad. Sci. USA* 100, 13567–13572.
- Anderson, D., Koch, C. A., Grey, L., Ellis, C., Moran, M. F., and Pawson, T. (1990). Binding of SH2 domains of phospholipase C gamma 1, GAP, and Src to activated growth factor receptors. *Science* 250, 979–982.
- Aoki, K., Nakamura, T., Fujikawa, K., and Matsuda, M. (2005). Local phosphatidylinositol 3,4,5-trisphosphate accumulation recruits Vav2 and Vav3 to activate Rac1/Cdc42 and initiate neurite outgrowth in nerve growth factor-stimulated PC12 cells. *Mol. Biol. Cell* 16, 2207–2217.
- Berrier, A. L., Mastrangelo, A. M., Downward, J., Ginsberg, M., and LaFlamme, S. E. (2000). Activated R-ras, Rac1, PI 3-kinase and PKCepsilon can each restore cell spreading inhibited by isolated integrin beta1 cytoplasmic domains. *J. Cell Biol.* 151, 1549–1560.
- Bretscher, M. S., and Aguado-Velasco, C. (1998). EGF induces recycling membrane to form ruffles. *Curr. Biol.* 8, 721–724.
- Cox, A. D., Bitva, T. R., Lowe, D. G., and Der, C. J. (1994). R-Ras induces malignant, but not morphologic, transformation of NIH3T3 cells. *Oncogene* 9, 3281–3288.
- Cozier, G. E., Bouyoucef, D., and Cullen, P. J. (2003). Engineering the phosphoinositide-binding profile of a class I pleckstrin homology domain. *J. Biol. Chem.* 278, 39489–39496.
- Feig, L. A. (1999). Tools of the trade: use of dominant-inhibitory mutants of Ras-family GTPases. *Nat. Cell Biol.* 1, E25–E27.
- Feig, L. A. (2003). Ral-GTPases: approaching their 15 minutes of fame. *Trends Cell Biol.* 13, 419–425.
- Finger, F. P., Hughes, T. E., and Novick, P. (1998). Sec3p is a spatial landmark for polarized secretion in budding yeast. *Cell* 92, 559–571.
- Friedrich, G. A., Hildebrand, J. D., and Soriano, P. (1997). The secretory protein Sec8 is required for paraxial mesoderm formation in the mouse. *Dev. Biol.* 192, 364–374.
- Furuhjelm, J., and Peranen, J. (2003). The C-terminal end of R-Ras contains a focal adhesion targeting signal. *J. Cell Sci.* 116, 3729–3738.
- Gildea, J. J., Harding, M. A., Seraj, M. J., Gulding, K. M., and Theodorescu, D. (2002). The role of Ral A in epidermal growth factor receptor-regulated cell motility. *Cancer Res.* 62, 982–985.
- Gonzalez-Garcia, A., Pritchard, C. A., Paterson, H. F., Mavria, G., Stamp, G., and Marshall, C. J. (2005). RalGDS is required for tumor formation in a model of skin carcinogenesis. *Cancer Cell* 7, 219–226.
- Gotoh, T., Niino, Y., Tokuda, M., Hatase, O., Nakamura, S., Matsuda, M., and Hattori, S. (1997). Activation of R-Ras by Ras-guanine nucleotide-releasing factor. *J. Biol. Chem.* 272, 18602–18607.
- Grindstaff, K. K., Yeaman, C., Anandasabapathy, N., Hsu, S. C., Rodriguez-Boulan, E., Scheller, R. H., and Nelson, W. J. (1998). Sec6/8 complex is recruited to cell-cell contacts and specifies transport vesicle delivery to the basal-lateral membrane in epithelial cells. *Cell* 93, 731–740.
- Gromley, A., Yeaman, C., Rosa, J., Redick, S., Chen, C. T., Mirabelle, S., Guha, M., Sillibourne, J., and Doherty, S. J. (2005). Centriolin anchoring of exocyst and SNARE complexes at the midbody is required for secretory-vesicle-mediated abscission. *Cell* 123, 75–87.
- Hamad, N. M., Elconin, J. H., Karnoub, A. E., Bai, W., Rich, J. N., Abraham, R. T., Der, C. J., and Counter, C. M. (2002). Distinct requirements for Ras oncogenesis in human versus mouse cells. *Genes Dev.* 16, 2045–2057.
- Hofer, F., Berdeaux, R., and Martin, G. S. (1998). Ras-independent activation of Ral by a Ca(2+)-dependent pathway. *Curr. Biol.* 8, 839–842.
- Huff, S. Y., Quilliam, L. A., Cox, A. D., and Der, C. J. (1997). R-Ras is regulated by activators and effectors distinct from those that control Ras function. *Oncogene* 14, 133–143.
- Inoue, M., Chang, L., Hwang, J., Chiang, S. H., and Saltiel, A. R. (2003). The exocyst complex is required for targeting of Glut4 to the plasma membrane by insulin. *Nature* 422, 629–633.
- Keely, P. J., Rusyn, E. V., Cox, A. D., and Parise, L. V. (1999). R-Ras signals through specific integrin alpha cytoplasmic domains to promote migration and invasion of breast epithelial cells. *J. Cell Biol.* 145, 1077–1088.
- Komatsu, M., and Ruoslahti, E. (2005). R-Ras is a global regulator of vascular regeneration that suppresses intimal hyperplasia and tumor angiogenesis. *Nat. Med.* 11, 1346–1350.
- Kurokawa, K., Itoh, R. E., Yoshizaki, H., Nakamura, T., and Matsuda, M. (2004a). Coactivation of Rac1 and Cdc42 at lamellipodia and membrane ruffles induced by epidermal growth factor. *Mol. Biol. Cell* 15, 1003–1010.
- Kurokawa, K., Takaya, A., Terai, K., Fujioka, A., and Matsuda, M. (2004b). Visualizing the signal transduction pathways in living cells with GFP-based FRET probes. *Acta Histochem. Cytochem.* 37, 347–355.
- Lim, K. H., Baines, A. T., Fioridalisi, J. J., Shipitsin, M., Feig, L. A., Cox, A. D., Der, C. J., and Counter, C. M. (2005). Activation of RalA is critical for Ras-induced tumorigenesis of human cells. *Cancer Cell* 7, 533–545.
- Lipschutz, J. H., and Mostov, K. E. (2002). Exocytosis: the many masters of the exocyst. *Curr. Biol.* 12, R212–R214.
- Lowe, D. G., Capon, D. J., Delwart, E., Sakaguchi, A. Y., Naylor, S. L., and Goeddel, D. V. (1987). Structure of the human and murine R-ras genes, novel genes closely related to ras proto-oncogenes. *Cell* 48, 137–146.
- Margolis, B., Li, N., Koch, A., Mohammadi, M., Hurwitz, D. R., Zilberstein, A., Ullrich, A., Pawson, T., and Schlessinger, J. (1990). The tyrosine phosphorylated carboxy terminus of the EGF receptor is a binding site for GAP and PLC-gamma. *EMBO J.* 9, 4375–4380.
- Marte, B. M., Rodriguez-Viciana, P., Wennstrom, S., Warne, P. H., and Downward, J. (1997). R-Ras can activate the phosphoinositide 3-kinase but not the MAP kinase arm of the Ras effector pathways. *Curr. Biol.* 7, 137–146.
- Matsuno, A., Mizutani, A., Itoh, J., Takekoshi, S., Nagashima, T., Okinaga, H., Takano, K., and Osamura, R. Y. (2005). Establishment of stable GH3 cell line expressing enhanced yellow fluorescent protein-growth hormone fusion protein. *J. Histochem. Cytochem.* 53, 1177–1180.
- Mochizuki, N., Yamashita, S., Kurokawa, K., Ohba, Y., Nagai, T., Miyawaki, A., and Matsuda, M. (2001). Spatio-temporal images of growth-factor-induced activation of Ras and Rap1. *Nature* 411, 1065–1068.
- Moskalenko, S., Henry, D. O., Rosse, C., Mirey, G., Camonis, J. H., and White, M. A. (2002). The exocyst is a Ral effector complex. *Nat. Cell Biol.* 4, 66–72.
- Moskalenko, S., Tong, C., Rosse, C., Mirey, G., Formstecher, E., Daviet, L., Camonis, J., and White, M. A. (2003). Ral GTPases regulate exocyst assembly through dual subunit interactions. *J. Biol. Chem.* 278, 51743–51748.
- Murthy, M., Garza, D., Scheller, R. H., and Schwarz, T. L. (2003). Mutations in the exocyst component Sec5 disrupt neuronal membrane traffic, but neurotransmitter release persists. *Neuron* 37, 433–447.
- Nagai, T., Ibat, K., Park, E. S., Kubota, M., Mikoshiba, K., and Miyawaki, A. (2002). A variant of yellow fluorescent protein with fast and efficient maturation for cell-biological applications. *Nat. Biotechnol.* 20, 87–90.
- Nakada, M., Niska, J. A., Tran, N. L., McDonough, W. S., and Berens, M. E. (2005). EphB2/R-Ras signaling regulates glioma cell adhesion, growth, and invasion. *Am. J. Pathol.* 167, 565–576.
- Nakashima, S., Morinaka, K., Koyama, S., Ikeda, M., Kishida, M., Okawa, K., Iwamatsu, A., Kishida, S., and Kikuchi, A. (1999). Small G protein Ral and its downstream molecules regulate endocytosis of EGF and insulin receptors. *EMBO J.* 18, 3629–3642.
- Nancy, V., Wolthuis, R. M., de Tand, M. F., Janoueix-Lerosey, I., Bos, J. L., and de Gunzburg, J. (1999). Identification and characterization of potential effector molecules of the Ras-related GTPase Rap2. *J. Biol. Chem.* 274, 8737–8745.

- Nishigaki, M., Aoyagi, K., Danjoh, I., Fukaya, M., Yanagihara, K., Sakamoto, H., Yoshida, T., and Sasaki, H. (2005). Discovery of aberrant expression of R-RAS by cancer-linked DNA hypomethylation in gastric cancer using microarrays. *Cancer Res.* 65, 2115–2124.
- Ohba, Y., Mochizuki, N., Yamashita, S., Chan, A. M., Schrader, J. W., Hattori, S., Nagashima, K., and Matsuda, M. (2000). Regulatory proteins of R-Ras, TC21/R-Ras2, and M-Ras/R-Ras3. *J. Biol. Chem.* 275, 20020–20026.
- Oinuma, I., Ishikawa, Y., Katoh, H., and Negishi, M. (2004). The Semaphorin 4D receptor Plexin-B1 is a GTPase activating protein for R-Ras. *Science* 305, 862–865.
- Oinuma, I., Katoh, H., and Negishi, M. (2006). Semaphorin 4D/Plexin-B1-mediated R-Ras GAP activity inhibits cell migration by regulating beta(1) integrin activity(2). *J. Cell Biol.* 173, 601–613.
- Oxford, G., Owens, C. R., Titus, B. J., Foreman, T. L., Herlevsen, M. C., Smith, S. C., and Theodorescu, D. (2005). RalA and RalB: antagonistic relatives in cancer cell migration. *Cancer Res.* 65, 7111–7120.
- Polzin, A., Shipitsin, M., Goi, T., Feig, L. A., and Turner, T. J. (2002). Ral-GTPase influences the regulation of the readily releasable pool of synaptic vesicles. *Mol. Cell. Biol.* 22, 1714–1722.
- Prigent, M., Dubois, T., Raposo, G., Derrien, V., Tenza, D., Rosse, C., Camonis, J., and Chavrier, P. (2003). ARF6 controls post-endocytic recycling through its downstream exocyst complex effector. *J. Cell Biol.* 163, 1111–1121.
- Proux-Gillardeaux, V., Gavard, J., Irinopoulou, T., Mege, R. M., and Galli, T. (2005). Tetanus neurotoxin-mediated cleavage of cellubrevin impairs epithelial cell migration and integrin-dependent cell adhesion. *Proc. Natl. Acad. Sci. USA* 102, 6362–6367.
- Quilliam, L. A., Rebhun, J. F., and Castro, A. F. (2002). A growing family of guanine nucleotide exchange factors is responsible for activation of Ras-family GTPases. *Prog. Nucleic Acid Res. Mol. Biol.* 71, 391–444.
- Rangarajan, A., Hong, S. J., Gifford, A., and Weinberg, R. A. (2004). Species- and cell type-specific requirements for cellular transformation. *Cancer Cell* 6, 171–183.
- Rey, L., Taylor-Harris, P., van Erp, H., and Hall, A. (1994). R-ras interacts with rasGAP, neurofibromin and c-raf but does not regulate cell growth or differentiation. *Oncogene* 9, 685–692.
- Rodriguez-Viciano, P., Sabatier, C., and McCormick, F. (2004). Signaling specificity by Ras family GTPases is determined by the full spectrum of effectors they regulate. *Mol. Cell. Biol.* 24, 4943–4954.
- Schmoranzler, J., Kreitzer, G., and Simon, S. M. (2003). Migrating fibroblasts perform polarized, microtubule-dependent exocytosis towards the leading edge. *J. Cell Sci.* 116, 4513–4519.
- Self, A. J., Caron, E., Paterson, H. F., and Hall, A. (2001). Analysis of R-Ras signalling pathways. *J. Cell Sci.* 114, 1357–1366.
- Shao, H., and Andres, D. A. (2000). A novel RalGEF-like protein, RGL3, as a candidate effector for rit and Ras. *J. Biol. Chem.* 275, 26914–26924.
- Shipitsin, M., and Feig, L. A. (2004). RalA but not RalB enhances polarized delivery of membrane proteins to the basolateral surface of epithelial cells. *Mol. Cell. Biol.* 24, 5746–5756.
- Spaargaren, M., and Bischoff, J. R. (1994). Identification of the guanine nucleotide dissociation stimulator for Ral as a putative effector molecule of R-ras, H-ras, K-ras, and Rap. *Proc. Natl. Acad. Sci. USA* 91, 12609–12613.
- Spaargaren, M., Martin, G. A., McCormick, F., Fernandez-Sarabia, M. J., and Bischoff, J. R. (1994). The Ras-related protein R-ras interacts directly with Raf-1 in a GTP-dependent manner. *Biochem. J.* 300, 303–307.
- Takaya, A., Ohba, Y., Kurokawa, K., and Matsuda, M. (2004). RalA activation at nascent lamellipodia of epidermal growth factor-stimulated Cos7 cells and migrating Madin-Darby canine kidney cells. *Mol. Biol. Cell* 15, 2549–2557.
- Tayeb, M. A., Skalski, M., Cha, M. C., Kean, M. J., Scaife, M., and Coppolino, M. G. (2005). Inhibition of SNARE-mediated membrane traffic impairs cell migration. *Exp. Cell Res.* 305, 63–73.
- Tsuboi, T., Ravier, M. A., Xie, H., Ewart, M. A., Gould, G. W., Baldwin, S. A., and Rutter, G. A. (2005). Mammalian exocyst complex is required for the docking step of insulin vesicle exocytosis. *J. Biol. Chem.* 280, 25565–25570.
- Vega, I. E., and Hsu, S. C. (2001). The exocyst complex associates with microtubules to mediate vesicle targeting and neurite outgrowth. *J. Neurosci.* 21, 3839–3848.
- Vitale, N., Mawet, J., Camonis, J., Regazzi, R., Bader, M. F., and Chasserot-Golaz, S. (2005). The Small GTPase RalA controls exocytosis of large dense core secretory granules by interacting with ARF6-dependent phospholipase D1. *J. Biol. Chem.* 280, 29921–29928.
- Wolthuis, R. M., and Bos, J. L. (1999). Ras caught in another affair: the exchange factors for Ral. *Curr. Opin. Genet. Dev.* 9, 112–117.
- Wozniak, M. A., Kwong, L., Chodniewicz, D., Klemke, R. L., and Keely, P. J. (2005). R-Ras controls membrane protrusion and cell migration through the spatial regulation of Rac and Rho. *Mol. Biol. Cell* 16, 84–96.
- Wu, S., Mehta, S. Q., Pichaud, F., Bellen, H. J., and Quioco, F. A. (2005). Sec15 interacts with Rab11 via a novel domain and affects Rab11 localization in vivo. *Nat. Struct. Mol. Biol.* 12, 879–885.
- Yamamoto, T., Matsui, T., Nakafuku, M., Iwamatsu, A., and Kaibuchi, K. (1995). A novel GTPase-activating protein for R-Ras. *J. Biol. Chem.* 270, 30557–30561.
- Yeaman, C., Grindstaff, K. K., Wright, J. R., and Nelson, W. J. (2001). Sec6/8 complexes on trans-Golgi network and plasma membrane regulate late stages of exocytosis in mammalian cells. *J. Cell Biol.* 155, 593–604.
- Zacharias, D. A., Violin, J. D., Newton, A. C., and Tsien, R. Y. (2002). Partitioning of lipid-modified monomeric GFPs into membrane microdomains of live cells. *Science* 296, 913–916.
- Zhang, X. M., Ellis, S., Sriratana, A., Mitchell, C. A., and Rowe, T. (2004). Sec15 is an effector for the Rab11 GTPase in mammalian cells. *J. Biol. Chem.* 279, 43027–43034.
- Zhang, Z., Vuori, K., Wang, H., Reed, J. C., and Ruoslahti, E. (1996). Integrin activation by R-ras. *Cell* 85, 61–69.

## Increased Endoplasmic Reticulum Stress in Atherosclerotic Plaques Associated With Acute Coronary Syndrome

Masafumi Myoishi, MD; Hiroyuki Hao, MD, PhD; Tetsuo Minamino, MD, PhD; Kouki Watanabe, MD, PhD; Kensaku Nishihira, MD, PhD; Kinta Hatakeyama, MD, PhD; Yujiro Asada, MD, PhD; Ken-ichiro Okada, MD, PhD; Hatsue Ishibashi-Ueda, MD, PhD; Giulio Gabbiani, MD, PhD; Marie-Luce Bochaton-Piallat, PhD; Naoki Mochizuki, MD, PhD; Masafumi Kitakaze, MD, PhD

**Background**—The endoplasmic reticulum (ER) responds to various stresses by upregulation of ER chaperones, but prolonged ER stress eventually causes apoptosis. Although apoptosis is considered to be essential for the progression and rupture of atherosclerotic plaques, the influence of ER stress and apoptosis on rupture of unstable coronary plaques remains unclear.

**Methods and Results**—Coronary artery segments were obtained at autopsy from 71 patients, and atherectomy specimens were obtained from 40 patients. Smooth muscle cells and macrophages in the fibrous caps of thin-cap atheroma and ruptured plaques, but not in the fibrous caps of thick-cap atheroma and fibrous plaques, showed a marked increase of ER chaperone expression and apoptotic cells. ER chaperones also showed higher expression in atherectomy specimens from patients with unstable angina pectoris than in specimens from those with stable angina. Expression of 7-ketocholesterol was increased in the fibrous caps of thin-cap atheroma compared with thick-cap atheroma. Treatment of cultured coronary artery smooth muscle cells or THP-1 cells with 7-ketocholesterol induced upregulation of ER chaperones and apoptosis, whereas these changes were prevented by antioxidants. We also investigated possible signaling pathways for ER-initiated apoptosis and found that the CHOP (a transcription factor induced by ER stress)-dependent pathway was activated in unstable plaques. In addition, knockdown of CHOP expression by small interfering RNA decreased ER stress-dependent death of cultured coronary artery smooth muscle cells and THP-1 cells.

**Conclusions**—Increased ER stress occurs in unstable plaques. Our findings suggest that ER stress-induced apoptosis of smooth muscle cells and macrophages may contribute to plaque vulnerability. (*Circulation*. 2007;116:1226-1233.)

**Key Words:** apoptosis ■ plaque ■ myocardial infarction ■ endoplasmic reticulum

Most of the acute clinical manifestations of coronary atherosclerosis result from plaque rupture that triggers thrombosis and vessel occlusion, producing the acute coronary syndrome (ACS).<sup>1-3</sup> Previous reports have shown that apoptosis affects all of the types of cells residing within atherosclerotic plaques, including smooth muscle cells (SMCs) and macrophages,<sup>4,5</sup> with oxidized low-density lipoprotein and several inflammatory factors being known to induce apoptosis.<sup>6,7</sup> The number of apoptotic cells depends on the plaque stage and is generally higher in more advanced plaques.<sup>6,8</sup> SMCs synthesize most of the interstitial collagen that stabilizes the fibrous cap of a plaque.<sup>4,7</sup> Therefore, excessive apoptosis of SMCs in the fibrous cap may compromise plaque integrity and render it

vulnerable to proteolytic attack by inflammatory cells, leading to plaque rupture.<sup>4,7</sup> Apoptotic macrophages are more frequent at sites of plaque rupture than in areas where the fibrous cap remains intact.<sup>9</sup> A decrease in macrophages would reduce the scavenging of apoptotic SMCs and macrophages, allowing the cells to undergo secondary necrosis, thereby increasing thrombogenicity of the plaque.<sup>10</sup>

Editorial p 1214

Clinical Perspective p 1233

The endoplasmic reticulum (ER) is 1 of the largest cellular organelles and has multiple functions, such as regulating the folding of proteins.<sup>11,12</sup> Various stimuli cause ER stress,

Received December 10, 2006; accepted July 6, 2007.

From the Departments of Cardiovascular Medicine (M.M., M.K.), Structural Analysis (M.M., N.M.), and Pathology (H.H., H.I.-U.), National Cardiovascular Center, Suita, Osaka, Japan; Department of Surgical Pathology (H.H.), Hyogo College of Medicine, Nishinomiya, Hyogo, Japan; Departments of Bioregulatory Medicine (M.M.) and Cardiovascular Medicine (T.M., K.-i.O.), Osaka University Graduate School of Medicine, Suita, Osaka, Japan; Division of Cardiology (K.W.), Uwajima City Hospital, Uwajima, Ehime, Japan; Department of Pathology (K.N., K.H., Y.A.), Faculty of Medicine, University of Miyazaki, Miyazaki, Japan; and Department of Pathology and Immunology (G.G., M.-L.B.-P.), University of Geneva-CMU, Geneva, Switzerland.

The online-only Data Supplement, consisting of expanded Methods, tables, and figures, is available with this article at <http://circ.ahajournals.org/cgi/content/full/CIRCULATIONAHA.106.682054/DC1>.

Correspondence to Masafumi Kitakaze, MD, PhD, Department of Cardiovascular Medicine, National Cardiovascular Center, Suita, Osaka 565-8565, Japan. E-mail [kitakaze@z66.so-net.ne.jp](mailto:kitakaze@z66.so-net.ne.jp)

© 2007 American Heart Association, Inc.

*Circulation* is available at <http://circ.ahajournals.org>

DOI: 10.1161/CIRCULATIONAHA.106.682054

Downloaded from [circ.ahajournals.org](http://circ.ahajournals.org) at National Cardiovascular Center on January 18, 2008

including ischemia, hypoxia, heat shock, mutation, increased protein synthesis, and reactive oxygen species, all of which can potentially lead to ER dysfunction.<sup>11,12</sup> In response to ER stress, there is marked upregulation of various ER chaperones, such as the 94-kDa glucose-regulated protein (GRP94) or GRP78 that stabilizes protein folding.<sup>11,13,14</sup> When the ER becomes overloaded with misfolded proteins, the unfolded protein response (UPR) occurs to enhance cell survival.<sup>15</sup> However, prolonged ER stress can trigger apoptotic cell death, which is promoted by transcriptional induction of C/EBP homologous protein (CHOP) and/or by the activation of c-JUN NH<sub>2</sub>-terminal kinase (JNK)- and/or caspase-12-dependent pathways.<sup>16</sup> In support of this concept, our investigation of the effects of prolonged ER stress on hypertrophic and failing hearts revealed that apoptosis of cardiac myocytes was induced via activation of CHOP, an ER-specific proapoptotic factor.<sup>17</sup> An important role of ER-initiated cell death pathways has also been demonstrated in several diseases, including diabetes mellitus,<sup>16</sup> neurodegenerative conditions,<sup>18</sup> and ischemia.<sup>19</sup>

Oxidation of low-density lipoprotein plays a significant pathogenic role in atherosclerosis.<sup>6,7,20</sup> In cultured peritoneal macrophages, excessive accumulation of free cholesterol (induced by acetyl low-density lipoprotein with an acyl-CoA:cholesterol acyltransferase [ACAT] inhibitor) initiates ER stress, increases CHOP expression, and leads to apoptosis.<sup>21</sup> Studies of apoE<sup>-/-</sup> mice also support the relevance of ER stress to macrophage apoptosis and to enlargement of the necrotic core in advanced atherosclerotic plaques.<sup>22,23</sup> However, it is still unclear whether ER stress and UPR activation have a role in plaque rupture. Unfortunately, the absence of a suitable animal model has greatly hindered investigation of the molecular mechanisms of plaque rupture and evaluation of the effects of ER stress *in vivo*.<sup>24,25</sup>

In the present study, we examined histological sections from atherosclerotic coronary artery lesions obtained at autopsy or after directional coronary atherectomy (DCA) to investigate markers of ER stress/UPR activation and apoptotic cell death. Oxysterols such as 7-ketocholesterol (7-KC) have been reported to be partially responsible for the cytotoxicity of oxidized low-density lipoprotein.<sup>26,27</sup> Exposure of cultured human SMCs to 7-KC induces the UPR and promotes apoptotic cell death,<sup>28</sup> so we investigated 7-KC expression in plaque specimens by immunohistochemistry. We also examined whether 7-KC could activate ER stress using cultured human coronary artery SMCs (CASMCs) and a monocyte cell line (THP-1). Furthermore, we investigated the possible signaling pathways for ER-initiated apoptosis, and we found that the CHOP (a transcription factor induced by ER stress)-dependent pathway was activated in unstable plaques, whereas knockdown of CHOP expression by small interfering RNA (siRNA) decreased ER stress-dependent death of cultured CASMCs and THP-1 cells.

## Methods

### Coronary Artery Specimens

Two different sets of specimens were obtained under a protocol approved by the Institutional Review Board of the National Cardiovascular Center and Miyazaki University. The first set of specimens

**TABLE 1. Human Coronary Specimens (Autopsy; n=71)**

Histological Classification of Lesions	No. of Specimens	AHA Classification
No. of specimens obtained at autopsy	152	...
Diffuse intimal thickening (normal)	21	Type I
Fibrous plaques (fibrous)	48	Type Vc
Thick-cap atheroma (thick)	51	Type Va
Thin-cap atheroma (thin)	15	Type Va
Ruptured plaques (ruptured)	17	Type VI

AHA Classification indicates American Heart Association histological criteria.<sup>30,31</sup>

was obtained at autopsy, and the second set was obtained by DCA. Classification of the histology of the lesions in autopsy specimens was done morphologically, as described previously (Table 1).<sup>29-31</sup> Demographic data for the study population are presented in Table I of the Data Supplement.

In brief, 152 coronary artery segments were obtained at autopsy from 71 patients, including 17 consecutive patients who experienced fatal ACS without percutaneous coronary intervention and 54 consecutive patients with noncardiac death. The major coronary arteries and their branches were cut transversely at ≈5-mm intervals, and 17 ruptured plaques were detected in the 17 ACS patients (ruptured: AHA type VI, n=17). The remaining 33 patients with noncardiac death and the 17 ACS patients also had advanced unruptured plaques (≥75% cross-sectional luminal narrowing), and we assessed each segment at the narrowest point (n=114). The advanced atherosclerotic unruptured plaques were additionally divided into fibrous plaques (fibrous: fibrocellular tissue was the predominant component, and the lipid core was inconspicuous or absent; AHA type Vc, n=48), thick-cap atheroma (thick: a lipid core covered by a fibrous cap >65-μm thick; AHA type Va, n=51), and thin-cap atheroma (thin: a lipid-rich core covered by a fibrous cap <65-μm thick<sup>32</sup>; AHA type Va, n=15). Another 21 patients with noncardiac death who had no advanced unruptured plaques and normal coronary arteries that only showed diffuse intimal thickening (normal: AHA type I, n=21) were used as a control group.

We performed a morphological analysis of multiple lesions (n=152) obtained at autopsy from 71 patients (Figure 1). The supplementary analyses included pairwise comparison of unruptured and ruptured plaques from each heart of each patient with ACS (Data Supplement Figure I) and investigation of the correlation between traditional cardiovascular risk factors and ER stress (Data Supplement Table II and Figure III). These supplementary analyses were based on representative data from each patient. (Details of the methods used to perform the supplementary analyses are included in the expanded Methods section in the Data Supplement.)

Forty DCA specimens were obtained from 40 patients who were treated for stable angina pectoris (SAP; n=20) or unstable angina pectoris (UAP; n=20). One DCA specimen was obtained per patient, and these specimens were classified on the basis of the clinical situation at the time of DCA (Table 2). These specimens were fixed in 4% paraformaldehyde for 6 hours at 4°C and then embedded in paraffin.

### Immunohistochemistry

Serial sections were examined by immunohistochemistry, as described previously.<sup>17</sup> In brief, sections were deparaffinized, and endogenous peroxidase activity was blocked by incubation with 0.3% H<sub>2</sub>O<sub>2</sub> in methanol for 30 minutes. For some antibodies, antigen retrieval was performed as specified below. After blocking with 3% normal bovine serum albumin, sections were incubated with the primary antibody overnight at 4°C. KDEL (Lys-Asp-Glu-Leu) antibody, which recognizes both GRP78 and GRP94, was purchased from Stressgen (San Diego, Calif) and was used at a dilution of 1:2000. Anti-CHOP antibody was obtained from Santa Cruz Biotechnology (Santa Cruz, Calif) and was applied at a dilution of 1:600

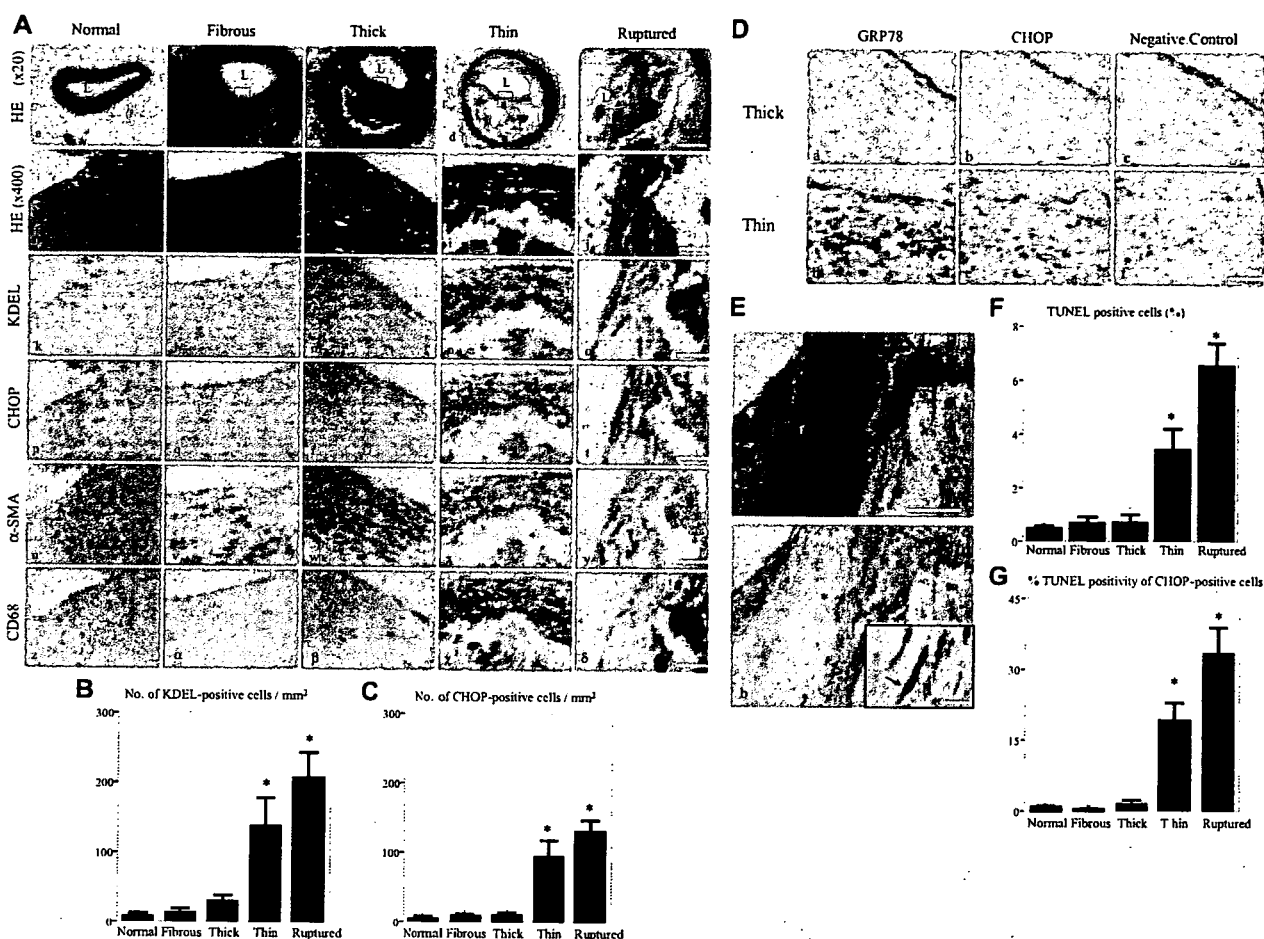


**Figure 1.** Induction of ER chaperones and death signals in coronary artery plaques obtained at autopsy. **A**, Comparison of hematoxylin-eosin (HE) staining, KDEL immunostaining, and CHOP immunostaining of normal arteries ( $n=14$ ), fibrous plaques ( $n=48$ ), thick-cap atheroma ( $n=51$ ), thin-cap atheroma ( $n=15$ ), and ruptured plaques ( $n=17$ ) obtained at autopsy from 71 patients. Representative HE-stained low-power micrographs from each group (a through e). L indicates the lumen, and the arrow shows the site of plaque rupture. The parts of the intima (a) and fibrous cap (b through e) indicated by boxes are shown at a higher magnification in panels f through j. Panels k through o show KDEL immunostaining. Panels p through t show CHOP immunostaining. Panels u through y show  $\alpha$ -smooth muscle actin ( $\alpha$ -SMA) immunostaining. Panels z through  $\delta$  show CD68 immunostaining. **B** and **C**, The number of KDEL-positive (**B**) and CHOP-positive (**C**) cells. The absolute number per square millimeter is shown for the media of a normal artery and for the fibrous caps of fibrous plaques, thick-cap atheroma, thin-cap atheroma, and ruptured plaques (**B**, **C**). **D**, ISH analysis of GRP78 (a, d), CHOP (b, e), and negative control (c, f) mRNA expression in thick- and thin-cap atheromas. **E**, Comparison of HE staining (a) with double immunostaining (b). Colocalization of CHOP (red) with TUNEL-positive cells (brown) in the cap of a ruptured plaque. The area indicated by asterisks is shown at a higher magnification in the inset. Arrows show CHOP and TUNEL double-positive cells. **F** and **G**, Percentage of TUNEL-positive cells (**F**) and percentage of TUNEL-positive cells among CHOP-positive cells (**G**) in the fibrous cap. Scale bars represent 1 mm (**A**, a through e), 50  $\mu$ m (**A**, f through  $\delta$ , **D**, and **E**), and 20  $\mu$ m (**E**, inset). \* $P<0.05$  vs normal plaque.

after antigen retrieval by incubation for 10 minutes at room temperature in 5  $\mu$ g/mL proteinase K. Anti-phospho-c-JUN NH<sub>2</sub>-terminal kinase antibody was used to detect c-JUN kinase (JNK), which is involved in the UPR.<sup>16</sup> It was obtained from Cell Signaling (Danvers, Mass) and was applied at a dilution of 1:100 after heat retrieval for 15 minutes at a sub-boiling temperature in 1 mmol/L EDTA (pH 8.0). Colon carcinoma sections were stained with anti-phospho-JNK antibody as a positive control. Anti- $\alpha$ -smooth muscle actin antibody and anti-human CD68 antibody (DAKO, Glostrup, Denmark) were used to identify SMCs and macrophages, respectively, and were used

at a dilution of 1:200. The EnVision kit (DAKO) was then used for immunostaining. Application of the KDEL antibody or the CHOP antibody after preincubation with each synthetic peptide used for immunization (KDEL: synthetic peptide SEKDEL, 10  $\mu$ g/mL, Tore Bio, CHOP peptide: 10  $\mu$ g/mL, Santa Cruz Biotechnology) resulted in no detectable signals, demonstrating the specificity of the antibody (Data Supplement Figure II).

### Terminal dUTP Nick End-Labeling Method and Double Immunohistochemistry

Cells undergoing apoptosis were identified by the terminal dUTP nick end-labeling (TUNEL) method with the ApopTag In Situ Apoptosis Detection Kit (Chemicon, Temecula, Calif), as described previously.<sup>8</sup> For simultaneous identification of CHOP and TUNEL immunoreactivity, double immunostaining of specimens was performed. First, the TUNEL method was performed with an ApopTag

**TABLE 2. Human Coronary Specimens (Atherectomy;  $n=40$ )**

Origin and Classification of Plaques	No. of Specimens
SAP	20
UAP	20

kit, and then CHOP was detected with an alkaline phosphatase-labeled secondary antibody with NewFukusin (DAKO).

### In Situ Hybridization

Digoxigenin-labeled cRNA probes and the negative control (LNE120) were purchased from Direct Communications Inc (Hiro-saki, Japan), and the sequences were as follows: GRP78: 5'-UGGAAUUCGAGUCGAGCCACCAACAAGAACAUUU-CAUCAUAUCAGACUUCUCAAUCAGAAUCUUCACAC-ACUUUCUGGACGGGCUUCAUAGUAGACCGGAACAGAU-CCA UGUUGAG-3'; CHOP: 5'-AUGCUCCAAUUGUUC AUG-CUUGGUGCAGAUUCACCAUUCGGUCAUUCAGAGCUCGG-CGAGUCGCCUCUACUUCUUCUUC-3'. In situ hybridization (ISH) was performed as described previously<sup>33</sup> with a Microprobe manual staining system (Fisher Scientific, Pittsburgh, Pa). In brief, hybridization of the probes (1 µg/mL) was performed for 120 minutes at 50°C, and then anti-digoxigenin-Ap (x250, Roche, Basel, Switzerland), as the secondary antibody, and NBT/BCIP stock solution (x50, Roche) were added.

### 7-KC Staining

Snap-frozen samples were obtained from 12 patients, comprising 6 with thick-cap atheroma and 6 with thin-cap atheroma. Frozen sections were fixed in 10% neutral-buffered formalin for 1 hour at room temperature. After blocking with 3% normal bovine serum albumin, the sections were incubated overnight at 4°C with anti-7-KC antibody (Nikken Seil Corporation, Fukuroi, Japan) at a dilution of 1:100, followed by incubation with an EnVision kit for 30 minutes.

### Statistical Analysis

Data are expressed as mean ± SEM. For the autopsy study of multiple lesions from many patients (Figure 1), statistical analysis was performed with the Kruskal-Wallis *H* test and a post hoc Mann-Whitney *U* test. For the DCA specimens, statistical analysis was performed with the Mann-Whitney *U* test. Experiments with cultured cells were performed at least 3 times each. Data obtained with cultured cells were analyzed statistically by the unpaired Student *t* test or ANOVA, followed by the Bonferroni test. Comparison of categorical variables was done with Fisher exact test. In all analyses, *P* < 0.05 was accepted as statistically significant. The expanded Methods section, covering supplementary data and in vitro studies is included as an online-only Data Supplement.

The authors had full access to and take full responsibility for the integrity of the data. All authors have read and agree to the manuscript as written.

## Results

### Upregulation of ER Chaperones and Apoptosis in the Fibrous Caps of Thin-Cap Atheroma and Ruptured Plaques

In the fibrous caps of thin-cap atheroma and ruptured plaques, KDEL and CHOP immunostaining showed a marked increase compared with the level of staining in the fibrous caps of thick-cap atheroma and fibrous plaques (Figure 1A k through t, Figure 1B, and Figure 1C). KDEL-positive cells were more numerous than CHOP-positive cells in the fibrous caps of thin-cap atheroma and ruptured plaques. Most of the CHOP-positive cells also expressed KDEL, as shown by staining of serial sections. In the same hearts of the ACS patients, there was a significant difference of KDEL- and CHOP-positive cells between the unruptured and ruptured plaques (Data Supplement Figure I). We also assessed ER chaperone (GRP78) and CHOP expression at the mRNA level by ISH (Figure 1D). Furthermore, we confirmed that the KDEL- and

CHOP-positive cells were SMCs or macrophages by immunostaining of serial sections with anti- $\alpha$ -smooth muscle actin and anti-CD68, respectively (Figure 1A, u through  $\delta$ ). In the fibrous caps of thin-cap atheroma and ruptured plaques, colocalization of CHOP immunoreactivity with TUNEL-positive cells was observed by double immunostaining (Figure 1E). The percentage of TUNEL-positive cells (Figure 1F) and the percentage of TUNEL-positive cells among CHOP-positive cells (Figure 1G) were increased compared with the findings in other specimens. Immunostaining for phospho-JNK, which is a proapoptotic factor involved in ER stress, revealed no immunoreactivity in the fibrous caps of thick, thin, or ruptured plaques (data not shown). In normal coronary artery specimens with diffuse intimal thickening (Figure 1A, k and p), there was no KDEL or CHOP positivity. In the region around the necrotic core of advanced plaques, KDEL positivity was only observed in macrophages. There was no significant difference in the number of KDEL-positive cells within the area surrounding the necrotic core of thick-cap atheromas ( $726 \pm 88/\text{mm}^2$ ), thin-cap atheromas ( $741 \pm 52/\text{mm}^2$ ), and ruptured plaques ( $651 \pm 102/\text{mm}^2$ ).

### Upregulation of ER Stress in Atherectomy Specimens From Patients With UAP

To estimate the activation of ER stress related to the clinical situation, we examined histological sections obtained at DCA. Morphometric analysis demonstrated that the number of KDEL- and CHOP-positive cells was significantly higher in patients with UAP than in patients with SAP (*P* < 0.05; Figures 2A, 2B, and 2C). The KDEL- and CHOP-positive cells were confirmed to be SMCs and macrophages (Figure 2A). When ER chaperone (GRP78) and CHOP mRNA levels were analyzed by quantitative reverse-transcription polymerase chain reaction or ISH, GRP78 expression was increased in patients with UAP (*P* = 0.14; Figure 2D), whereas CHOP expression was significantly higher in UAP patients than in SAP patients (*P* < 0.05; Figure 2E). On the other hand, both GRP78 and CHOP were significantly increased according to ISH (Figure 2F), but we could not confirm a significant increase of GRP78 by reverse-transcription polymerase chain reaction. This may have been because the number of fresh DCA specimens was too low.

### Immunohistochemical Detection of 7-KC in the Fibrous Caps of Atherosclerotic Plaques

To explore the likely molecular mechanism of activation of ER stress and the mechanistic link to apoptosis, we investigated plaque lipids by staining frozen coronary artery sections with anti-7-KC antibody (Figure 3), and the in vitro studies were performed (Figure 4). Immunoreactivity for 7-KC was increased in the fibrous caps of thin-cap atheroma, whereas no immunoreactivity was detected in the fibrous caps of thick-cap atheroma (Figure 3). In the region around the lipid core, however, 7-KC immunoreactivity was visible in both types of atheroma (Figure 3).

**Upregulation of ER Chaperones, CHOP, and Apoptosis by 7-KC and Effects of CHOP Knockdown by siRNA in CSMCs or THP-1 Cells**  
Exposure of cells to 7-KC increased the expression of GRP78 and CHOP mRNA, whereas this increase was prevented by



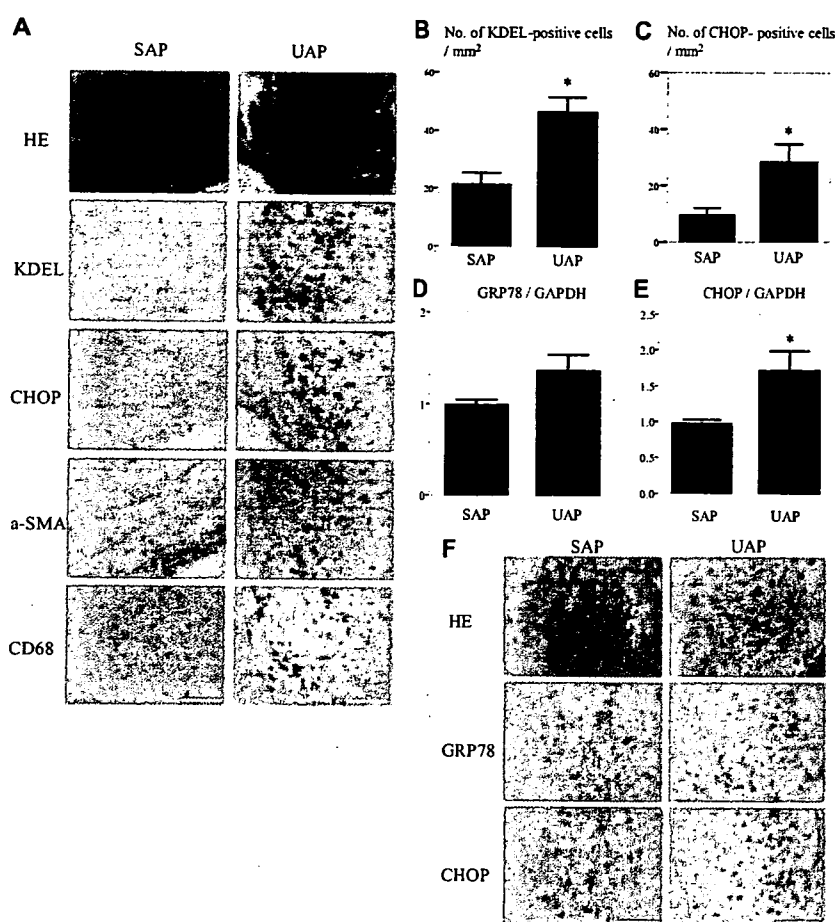


**Figure 2.** Induction of ER chaperones and death signals in atherectomy specimens obtained from the culprit lesions of patients with UAP. A, Comparison of hematoxylin-eosin (HE) staining with KDEL, CHOP,  $\alpha$ -smooth muscle actin ( $\alpha$ -SMA), and CD68 immunostaining of the serial sections of 32 atherectomy specimens obtained from patients with SAP (n=16) or UAP (n=16). B and C, Number of KDEL-positive (B) and CHOP-positive (C) cells per square millimeter. D and E, Comparison of GRP78 and CHOP expression normalized for GAPDH in 8 specimens from patients with SAP (n=4) or UAP (n=4) by quantitative reverse-transcription polymerase chain reaction. F, HE staining and ISH analysis of GRP78 (a, d) and CHOP (b, e) mRNA expression in specimens from SAP patients (n=6) or UAP patients (n=6). Scale bar represents 50  $\mu$ m. \* $P$ <0.05 vs SAP.

the antioxidants *N*-acetylcysteine or glutathione (Figure 4A). We observed intracellular production of reactive oxygen species after exposure to 7-KC, whereas glutathione reduced reactive oxygen species production (Figure 4B). We also

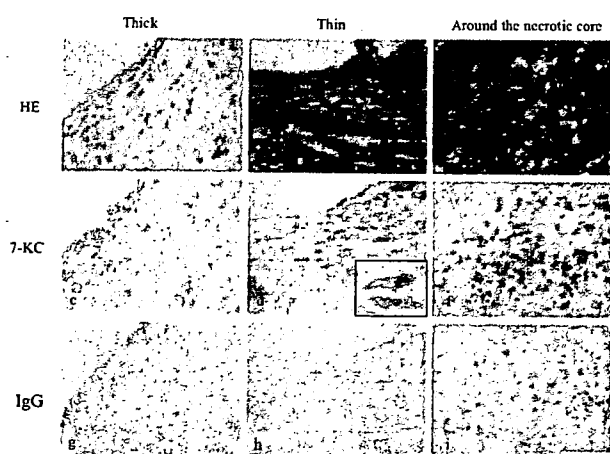


**Figure 3.** Immunohistochemical detection of 7-KC in the fibrous cap of thin-cap atheroma. Comparison of hematoxylin-eosin (HE) staining with 7-KC or IgG immunostaining in the fibrous caps of thick-cap atheroma (n=6) and thin-cap atheroma (n=6), as well as around the necrotic core of thick-cap atheroma. 7-KC immunostaining is shown at a higher magnification in the inset. Scale bar represents 50  $\mu$ m.

examined the effects of 7-KC on apoptosis of CASCs and THP-1 cells (Figure 4C). Treatment with 7-KC increased FITC-annexin and propidium iodide staining in a dose-dependent (Figure 4C, b and c) and time-dependent (data not shown) manner. Treatment of CASCs and THP-1 cells with 7-KC for 24 hours also induced apoptosis along with the induction of ER chaperones and CHOP at the protein level (Figure 4D). When CASCs and THP-1 cells were simultaneously incubated with 7-KC and *N*-acetylcysteine or glutathione, both antioxidants reduced the induction of ER chaperones (Figure 4D). Quantitative analysis revealed that most of the CHOP-positive cells coexpressed KDEL (88.2% of CHOP-positive CASCs and 72.7% of CHOP-positive THP-1 cells;  $P$ <0.05, Fisher's exact test), whereas there were few KDEL-negative and CHOP-positive cells, which suggests that CHOP was involved in the mediation of ER-initiated signaling (Figure 4D, c and d). Treatment of THP-1 cells with 7-KC induced CHOP, whereas 2 different siRNAs targeting CHOP caused the knockdown of CHOP expression (Figure 4E, a). Knockdown of CHOP expression by siRNA decreased the number of TUNEL-positive THP-1 cells after exposure to 7-KC (Figure 4E, b and d). Similarly, the knockdown of CHOP expression by siRNA decreased the number of TUNEL-positive CASCs after exposure to 7-KC (Figure 4E, c).



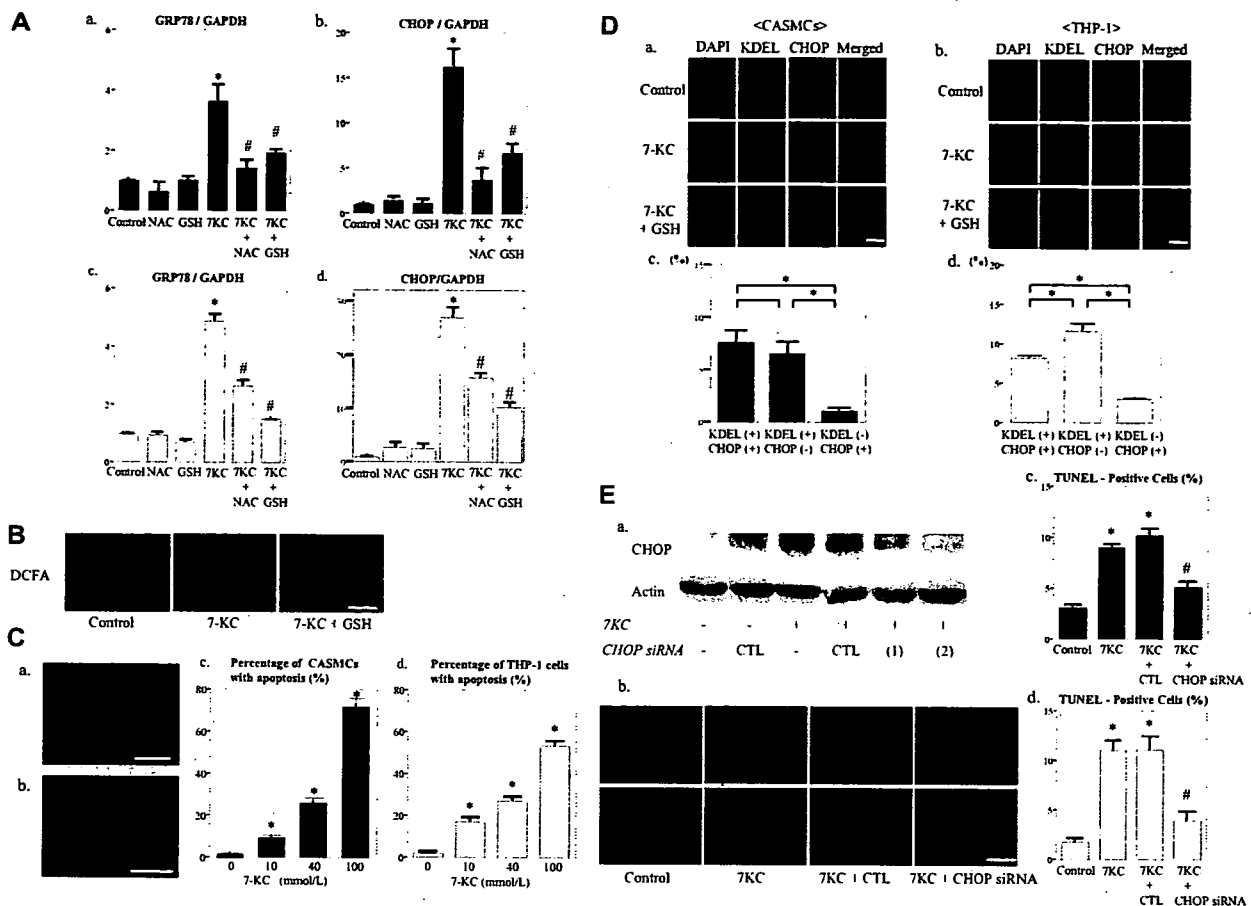


**Figure 4.** Upregulation of ER chaperones, CHOP, and apoptosis by exposure to 7-KC and effect of CHOP knockdown by siRNA in cultured CASCs or THP-1 cells. **A**, Comparison of GRP78 and CHOP expression normalized for GAPDH by quantitative reverse-transcription polymerase chain reaction. CASCs or THP-1 cells were incubated with 7-KC (80 mmol/L) in the absence or presence of *N*-acetylcysteine (NAC) or glutathione (GSH) for 12 hours. **B**, Measurement of reactive oxygen species (ROS) generation after exposure to 7-KC and 2', 7'-dichlorofluorescein diacetate (DCFH-DA) in the absence or presence of GSH for 12 hours. **C**, FITC-annexin V and propidium iodide staining for apoptosis of CASCs and THP-1 cells incubated with 7-KC (a). Exposure to 7-KC induced apoptosis of CASCs (b) and THP-1 cells (c) in a dose-dependent manner. **D**, KDEL and CHOP staining of CASCs (a) and THP-1 cells (b) after incubation with 7-KC in the absence or presence of GSH for 24 hours; c and d, quantitative analysis of immunohistochemical staining of CASCs (c) and THP-1 cells (d). **E**, Western blotting for CHOP after exposure to 7-KC with or without CHOP siRNA (a). TUNEL staining of THP-1 cells (b) and quantitative analysis of TUNEL-positive CASCs (c) and THP-1 cells (d). CTL indicates the nonsilenced control. Scale bars represent 50  $\mu$ m (B, C, and E) and 20  $\mu$ m (D). \* $P$ <0.05 vs control (A, C, and E). # $P$ <0.05 vs treatment with 7-KC (E). Experiments were performed at least 3 times. The data are expressed as mean  $\pm$  SEM. The immunofluorescent staining and Western blotting data are representative of at least 3 independent experiments.

## Discussion

The present study revealed a marked increase of ER chaperone expression, CHOP expression, and apoptosis in the fibrous caps of thin-cap atheroma or ruptured plaques, as well as in atherectomy specimens from UAP patients, which suggests that ER stress may play a role in the progression of plaque vulnerability and the occurrence of acute complications of coronary atherosclerosis in humans. Because of the inherent limitations of an autopsy study, we could not exclude the possibility that UPR activation occurred after plaque rupture. Previous reports have shown that ER chaperones, such as GRP78 or GRP94, may have a protective effect against ischemia/reperfusion injury.<sup>34</sup> However, the presence of apoptotic changes in the thin-cap atheroma of the patients with noncardiac death suggested that the findings we observed in ruptured plaques represented the evolution of such

changes in the thin-cap atheroma rather than being secondary to plaque rupture or ischemia/reperfusion injury. Only specimens from patients without percutaneous coronary intervention were studied, to exclude the influence of this intervention. We also observed an increase of ER stress-related changes in freshly fixed atherectomy specimens obtained from UAP patients compared with those from SAP patients. This suggests that ER stress activation was related to the clinical situation, and the autopsy specimens were only slightly affected by postmortem protein degradation.

Among the oxysterols, 7-KC is most frequently detected at high levels in atherosclerotic plaques and in the plasma of patients with a high cardiovascular risk.<sup>26,35</sup> To the best of our knowledge, however, 7-KC has not previously been detected in human atherosclerotic coronary artery sections by immunohistochemistry. It has been reported that 7-KC induces the

production of reactive oxygen species, activation of the UPR, and induction of apoptotic death in cultured human SMCs.<sup>28</sup> We demonstrated that the fibrous caps of thin-cap atheroma were immunohistochemically positive for 7-KC, a finding consistent with the increase of ER stress/UPR markers.

Treatment of CASMCs with 7-KC induced ER stress and activation of the UPR, findings that were consistent with the results of a previous study on aortic SMCs,<sup>28</sup> and these changes also occurred in THP-1 cells. This 7-KC-induced cellular damage was prevented by antioxidants (*N*-acetylcysteine and glutathione), which was also consistent with a previous report.<sup>36</sup> Accordingly, the present findings suggest that an increase of ER stress due to 7-KC induces apoptosis of SMCs and macrophages through the production of reactive oxygen species.

ER stress induces apoptosis via the CHOP-, JNK-, and caspase-12-dependent signaling pathways.<sup>16</sup> CHOP is mainly induced at the transcriptional level by ER stress,<sup>12,37</sup> after which its overexpression leads to apoptosis.<sup>11,16,38</sup> CHOP knockout mice show normal development and normal fertility but exhibit less apoptosis in response to ER stress.<sup>16,21</sup> Thus, detection of the induction of CHOP indicates an increase of ER-initiated apoptosis. Although the direct transcriptional target of CHOP has not been found,<sup>39</sup> the Bcl-2 pathway may be involved in the downstream connection between CHOP and apoptosis.<sup>28,39</sup> Caspase-12 is only activated by ER stress.<sup>13,16,18</sup> Although caspase-12 has been cloned in mice and rats, it is not yet possible to explore the role of this caspase in humans.<sup>40</sup> JNK is 1 of the stress-activated protein kinases that has been shown to induce apoptosis in response to ER stress.<sup>13,16</sup> We demonstrated that TUNEL-positive SMCs and macrophages were significantly increased in the fibrous cap, with CHOP (but not JNK) being induced simultaneously. Treatment of CASMCs or THP-1 cells with 7-KC induced CHOP, whereas knockdown of CHOP expression by siRNA led to a decrease of TUNEL-positive cells after exposure to 7-KC. Because CHOP is a transcription factor that specifically mediates ER-initiated apoptosis, the induction of CHOP in ruptured and unstable plaques supports the activation of ER-initiated apoptosis. However, our autopsy study could not exclude the possibility that the cells underwent apoptosis independently of CHOP, whereas the TUNEL assay gave false-positive results in the clinical specimens.

Unfortunately, we could not confirm whether or not the relationship between thinning of the fibrous cap and ER stress was causative because of the lack of a suitable animal model of plaque rupture. On the other hand, together with the present finding that 7-KC induced ER stress, the possibility that ER stress causes plaque vulnerability is also supported by the following reports. In cultured peritoneal macrophages, excessive accumulation of free cholesterol has been found to initiate ER stress, increase CHOP expression, and increase apoptosis.<sup>21</sup> Moreover, in vivo studies with apoE<sup>-/-</sup> mice have shown that lesional necrosis can be diminished by a decrease in the cholesterol level.<sup>22</sup> In addition, the present study demonstrated that expression of ER chaperones was upregulated to a similar extent in macrophages surrounding the necrotic cores of thick-cap atheroma, thin-cap atheroma,

and ruptured plaques, which suggests that ER stress may contribute to the progression of plaque vulnerability by inducing macrophage apoptosis.

In conclusion, the present findings support the possibility that ER stress and/or the UPR induces apoptosis of SMCs and macrophages, thus increasing the vulnerability of coronary artery plaques, which may lead to ACS and a fatal outcome in patients with coronary artery disease.

### Acknowledgments

We thank Akiko Ogai, Tomoko Morita, and Kazuyoshi Masuda for their technical assistance and Akiko Kada and Nobuo Shirahashi for their statistical advice.

### Sources of Funding

The present study was supported by a grant from the Japan Cardiovascular Research Foundation and a research grant for cardiovascular disease (14C-4) from the Japanese Ministry of Health, Labor and Welfare.

### Disclosures

None.

### References

1. Fuster V, Lewis A. Conner Memorial Lecture: mechanisms leading to myocardial infarction: insights from studies of vascular biology. *Circulation*. 1994;90:2126–2146.
2. Lee RT, Libby P. The unstable atheroma. *Arterioscler Thromb Vasc Biol*. 1997;17:1859–1867.
3. Falk E, Shah PK, Fuster V. Coronary plaque disruption. *Circulation*. 1995;92:657–671.
4. Bennett MR. Apoptosis of vascular smooth muscle cells in vascular remodeling and atherosclerotic plaque rupture. *Cardiovasc Res*. 1999;41:361–368.
5. Bjorkerud S, Bjorkerud B. Apoptosis is abundant in human atherosclerotic lesions, especially in inflammatory cells (macrophages and T cells), and may contribute to the accumulation of gruel and plaque instability. *Am J Pathol*. 1996;149:367–380.
6. Littlewood TD, Bennett MR. Apoptotic cell death in atherosclerosis. *Curr Opin Lipidol*. 2003;14:469–475.
7. Lindstedt KA, Leskinen MJ, Kovanen PT. Proteolysis of the pericellular matrix: a novel element determining cell survival and death in the pathogenesis of plaque erosion and rupture. *Arterioscler Thromb Vasc Biol*. 2004;24:1350–1358.
8. Kockx MM, De Meyer GR, Muhring J, Jacob W, Bult H, Herman AG. Apoptosis and related proteins in different stages of human atherosclerotic plaques. *Circulation*. 1998;97:2307–2315.
9. Kolodgie FD, Narula J, Burke AP, Haider N, Farb A, Hui-Liang Y, Smialek J, Virmani R. Localization of apoptotic macrophages at the site of plaque rupture in sudden coronary death. *Am J Pathol*. 2000;157:1259–1268.
10. Stoneman V, Bennet MR. Role of apoptosis in atherosclerosis and its therapeutic implications. *Clin Sci*. 2004;107:343–354.
11. Kaufman RJ. Stress signaling from the lumen of the endoplasmic reticulum: coordination of gene transcriptional and translational controls. *Genes Dev*. 1999;13:1211–1233.
12. Ron D. Translational control in the endoplasmic reticulum stress response. *J Clin Invest*. 2002;110:1383–1388.
13. Ferri KF, Kroemer G. Organelle-specific initiation of cell death pathways. *Nat Cell Biol*. 2001;3:E255–E263.
14. Patterson C, Cyr D. Welcome to the machine: a cardiologist's introduction to protein folding and degradation. *Circulation*. 2002;106:2741–2746.
15. Mori K. Tripartite management of unfolded proteins in the endoplasmic reticulum. *Cell*. 2000;101:451–454.
16. Oyadomari S, Araki E, Mori M. Endoplasmic reticulum stress-mediated apoptosis in pancreatic beta-cells. *Apoptosis*. 2002;7:335–345.
17. Okada K, Minamino T, Tsukamoto Y, Liao Y, Tsukamoto O, Takashima S, Hirata A, Fujita M, Nagamachi Y, Nakatani T, Yutani C, Ozawa K, Ogawa S, Tomoike H, Hori M, Kitakaze M. Prolonged endoplasmic

- reticulum stress in hypertrophic and failing heart after aortic constriction. *Circulation*. 2004;110:705–712.
18. Nakagawa T, Zhu H, Morishima N, Li E, Xu J, Yankner BA, Yuan J. Caspase-12 mediates endoplasmic-reticulum-specific apoptosis and cytotoxicity by amyloid-beta. *Nature*. 2000;403:98–103.
  19. Little E, Tocco G, Baudry M, Lee AS, Schreiber SS. Induction of glucose-regulated protein (glucose-regulated protein 78/BiP and glucose-regulated protein 94) and heat shock protein 70 transcripts in the immature rat brain following status epilepticus. *Neuroscience*. 1996;75:209–219.
  20. Ross R. Atherosclerosis: an inflammatory disease. *N Engl J Med*. 1999;340:115–126.
  21. Feng B, Yao PM, Li Y, Devlin CM, Zhang D, Harding HP, Sweeney M, Rong JX, Kuriakose G, Fisher EA, Marks AR, Ron D, Tabas I. The endoplasmic reticulum is the site of cholesterol-induced cytotoxicity in macrophages. *Nat Cell Biol*. 2003;5:781–792.
  22. Feng B, Zhang D, Kuriakose G, Devlin CM, Kockx M, Tabas I. Niemann-Pick C heterozygosity confers resistance to lesional necrosis and macrophage apoptosis in murine atherosclerosis. *Proc Natl Acad Sci U S A*. 2003;100:10423–10428.
  23. Zhou J, Lhoták S, Hilditch BA, Austin RC. Activation of unfolded protein response occurs at all stages of atherosclerotic lesion development in apolipoprotein E-deficient mice. *Circulation*. 2005;111:1814–1821.
  24. Cullen P, Baetta R, Bellostà S, Bernini F, Chinetti G, Cignarella A, von Eckardstein A, Exley A, Goddard M, Hofker M, Hurt-Camejo E, Kanters E, Kovanen P, Lorkowski S, McPheat W, Pentikainen M, Rauterberg J, Ritchie A, Staels B, Weikamp B, de Winther M; for the MAFAPS Consortium. Rupture of the atherosclerotic plaque: does a good animal model exist? *Arterioscler Thromb Vasc Biol*. 2003;23:535–542.
  25. Lutgens E, Suylen R, Faber BC, Gijbels MJ, Eurlings PM, Bijlens AP, Cleutjens KB, Heeneman S, Daemen MJ. Atherosclerotic plaque rupture: local or systemic process? *Arterioscler Thromb Vasc Biol*. 2003;23:2123–2130.
  26. Brown AJ, Jessup W. Oxysterols and atherosclerosis. *Atherosclerosis*. 1999;142:1–28.
  27. Bjorkhem I, Diczfalusy U. Oxysterols: friends, foes, or just fellow passengers? *Arterioscler Thromb Vasc Biol*. 2002;22:734–742.
  28. Pedruzzi E, Guichard C, Ollivier V, Driss F, Fay M, Prunet C, Marie JC, Pouzet C, Samadi M, Elbim C, O'Dowd Y, Bens M, Vandewalle A, Gougerot-Pocidallo MA, Lizard G, Ogier-Denis E. NAD(P)H oxidase Nox-4 mediates 7-ketocholesterol-induced endoplasmic reticulum stress and apoptosis in human aortic smooth muscle cells. *Mol Cell Biol*. 2004;24:10703–10717.
  29. Naruko T, Ueda M, Haze K, van der Wal AC, van der Loos CM, Itoh A, Komatsu R, Ikura Y, Ogami M, Shimada Y, Ehara S, Yoshiyama M, Takeuchi K, Yoshikawa J, Becker AE. Neutrophil infiltration of culprit lesions in acute coronary syndromes. *Circulation*. 2002;106:2894–2900.
  30. Stary HC, Chandler AB, Glagov S, Guyton JR, Insull W Jr, Rosenfeld ME, Schaffer A, Schwartz CJ, Wagner WD, Wissler RW. A definition of initial, fatty streak, and intermediate lesions of atherosclerosis. *Arterioscler Thromb*. 1994;14:840–856.
  31. Stary HC, Chandler AB, Dinsmore RE, Fuster V, Glagov S, Insull W, Rosenfeld ME, Schwartz CJ, Wagner WD, Wissler RW. A definition of advanced types of atherosclerotic lesions and a histological classification of atherosclerosis. *Arterioscler Thromb Vasc Biol*. 1995;15:1512–1531.
  32. Kolodgie FD, Burke AP, Farb A, Gold HK, Yuan J, Narula J, Finn AV, Virmani R. The thin-cap fibroatheroma: a type of vulnerable plaque: the major precursor lesion to acute coronary syndromes. *Curr Opin Cardiol*. 2001;16:285–292.
  33. Kuniyasu H, Ukai R, Johnston D, Troncoso P, Fidler IJ, Pettaway CA. The relative mRNA expression levels of matrix metalloproteinase to E-cadherin in prostate biopsy specimens distinguishes organ-confined from advanced prostate cancer at radical prostatectomy. *Clin Cancer Res*. 2003;9:2185–2194.
  34. Martindale JJ, Fernandez R, Thuerauf D, Whittaker R, Gude N, Sussman MA, Glembocki CC. Endoplasmic reticulum stress gene induction and protection from ischemia/reperfusion injury in the hearts of transgenic mice with a tamoxifen-regulated form of ATF6. *Circ Res*. 2006;98:1186–1193.
  35. Zhou Q, Wasowicz E, Handler B, Fleischer L, Kummerow FA. An excess concentration of oxysterols in the plasma is cytotoxic to cultured endothelial cells. *Atherosclerosis*. 2000;149:191–197.
  36. Lizard G, Guedry S, Sordet O, Monier S, Athias A, Mignet C, Bessede G, Lemaire S, Solary E, Gamber P. Glutathione is implied in the control of 7-ketocholesterol-induced apoptosis, which is associated with radical oxygen species production. *FASEB J*. 1998;12:1651–1663.
  37. Wang XZ, Lawson B, Brewer JW, Zinsner H, Sanjay A, Mi LJ, Boorstein R, Kreibich G, Hendershot LM, Ron D. Signals from the stressed endoplasmic reticulum induce C/EBP-homologous protein (CHOP/GADD153). *Mol Cell Biol*. 1996;16:4273–4280.
  38. Barone MV, Crozat A, Tabae A, Philipson L, Ron D. CHOP (GADD153) and its oncogenic variant, TLSCHP, have opposing effects on the induction of G1/S arrest. *Genes Dev*. 1994;8:453–464.
  39. Oyadomari S, Mori M. Roles of CHOP/GADD153 in endoplasmic reticulum stress. *Cell Death Differ*. 2004;11:381–389.
  40. Fischer H, Koenig U, Eckhart L, Tschachler E. Human caspase 12 has acquired deleterious mutations. *Biochem Biophys Res Commun*. 2002;293:722–772.

### CLINICAL PERSPECTIVE

Most of the acute clinical manifestations of coronary atherosclerosis result from plaque rupture that produces the acute coronary syndrome, and apoptosis is considered to be essential for plaque rupture. The endoplasmic reticulum (ER) is 1 of the largest cellular organelles and has multiple functions, such as regulating the folding of proteins. Various stimuli cause ER stress, including ischemia, heat shock, mutation, increased protein synthesis, and reactive oxygen species, all of which can potentially lead to ER dysfunction. The ER responds to stresses by upregulation of ER chaperones, but prolonged ER stress eventually causes apoptosis. However, the influence of ER stress and apoptosis on rupture of unstable coronary plaques remains unclear. We examined histological sections from coronary artery segments obtained at autopsy from 71 patients and atherectomy specimens obtained from 40 patients. Smooth muscle cells and macrophages in the fibrous caps of thin-cap atheroma and ruptured plaques showed a marked increase of ER chaperone expression and apoptotic cells. ER chaperones also showed higher expression in atherectomy specimens from patients with unstable angina pectoris than from those with stable angina. We also investigated possible signaling pathways for ER-initiated apoptosis and found that the C/EBP homologous protein (a transcription factor induced by ER stress)-dependent pathway was activated in unstable plaques. In addition, knockdown of C/EBP homologous protein expression by small interfering RNA decreased ER stress-dependent death of cultured coronary artery smooth muscle cells and THP-1 cells. Increased ER stress occurs in unstable plaques. Our findings suggest that ER stress-induced apoptosis may contribute to plaque vulnerability.



# A cardiac myosin light chain kinase regulates sarcomere assembly in the vertebrate heart

Osamu Seguchi,<sup>1</sup> Seiji Takashima,<sup>2,3</sup> Satoru Yamazaki,<sup>1</sup> Masanori Asakura,<sup>1</sup> Yoshihiro Asano,<sup>2</sup> Yasunori Shintani,<sup>2</sup> Masakatsu Wakeno,<sup>1</sup> Tetsuo Minamino,<sup>2</sup> Hiroya Kondo,<sup>2</sup> Hidehiko Furukawa,<sup>4</sup> Kenji Nakamaru,<sup>4</sup> Asuka Naito,<sup>4</sup> Tomoko Takahashi,<sup>4</sup> Toshiaki Ohtsuka,<sup>4</sup> Koichi Kawakami,<sup>5</sup> Tadashi Isomura,<sup>6</sup> Soichiro Kitamura,<sup>1</sup> Hitonobu Tomoike,<sup>1</sup> Naoki Mochizuki,<sup>1</sup> and Masafumi Kitakaze<sup>1</sup>

<sup>1</sup>Department of Cardiovascular Medicine, National Cardiovascular Center, Suita, Osaka, Japan. <sup>2</sup>Department of Cardiovascular Medicine and <sup>3</sup>Health Care Center, Osaka University Graduate School of Medicine, Suita, Osaka, Japan. <sup>4</sup>Core Technology Research Laboratories, Sankyo Co. Ltd., Shinagawa, Tokyo, Japan. <sup>5</sup>Division of Molecular and Developmental Biology, National Institute of Genetics, Mishima, Shizuoka, Japan. <sup>6</sup>Hayama Heart Center, Hayama, Kanagawa, Japan.

**Marked sarcomere disorganization is a well-documented characteristic of cardiomyocytes in the failing human myocardium. Myosin regulatory light chain 2, ventricular/cardiac muscle isoform (MLC2v), which is involved in the development of human cardiomyopathy, is an important structural protein that affects physiologic cardiac sarcomere formation and heart development. Integrated cDNA expression analysis of failing human myocardia uncovered a novel protein kinase, cardiac-specific myosin light chain kinase (cardiac-MLCK), which acts on MLC2v. Expression levels of cardiac-MLCK were well correlated with the pulmonary arterial pressure of patients with heart failure. In cultured cardiomyocytes, knockdown of cardiac-MLCK by specific siRNAs decreased MLC2v phosphorylation and impaired epinephrine-induced activation of sarcomere reassembly. To further clarify the physiologic roles of cardiac-MLCK in vivo, we cloned the zebrafish ortholog  $\alpha$ -cardiac-MLCK. Knockdown of  $\alpha$ -cardiac-MLCK expression using morpholino antisense oligonucleotides resulted in dilated cardiac ventricles and immature sarcomere structures. These results suggest a significant role for cardiac-MLCK in cardiogenesis.**

## Introduction

Despite recent advances in pharmacologic and surgical therapies, chronic heart failure (CHF) is still a leading cause of death worldwide (1). Currently, heart transplant is thought to be the most effective therapy for end-stage CHF. However, this approach obviously cannot be used for all of the numerous affected patients and is not suitable for patients with a mild disease state. Therefore, there is increasing demand for new therapeutic targets for CHF.

Cardiomyocytes, the most basic cellular unit of the myocardium, express several sarcomeric proteins, including myosin and actin; abnormalities in these sarcomeric proteins are major causes of idiopathic cardiomyopathies and lead to CHF (2-4). Type II myosin is the major constituent of sarcomeres. In the neck region of this protein, there are binding sites for a pair of myosin light chains, which are called the essential light chain and the regulatory light chain. Among the several paralogs of the myosin regulatory light chain in vertebrates (5), myosin regulatory light chain 2, ventricular/cardiac muscle isoform (MLC2v) is expressed in the myocardium, where it performs specific roles in cardiogenesis by contributing to the for-

mation of sarcomeres and in increasing the Ca<sup>2+</sup> sensitivity of muscle tension at submaximal Ca<sup>2+</sup> concentrations (6, 7). Currently, 2 members of the myosin light chain kinase (MLCK) protein family that act on myosin regulatory light chain in muscle cells have been identified, skeletal muscle MLCK (skMLCK) and smooth muscle MLCK (smMLCK) (8). Among these MLCK family members, smMLCK, including nonmuscle isoforms, is distributed ubiquitously in various tissues and contributes to the contraction of smooth muscle and several cell activities. Conversely, skMLCK is thought to localize and function in both cardiac muscle and skeletal muscle (9); to our knowledge, no cardiac-specific MLCK has been reported to date. skMLCK-deficient mice, however, did not show any heart weight, body weight, or heart weight/body weight ratio phenotypes, despite effective knockdown of skMLCK expression (10). Additionally, there were no significant differences between the knockout and wild-type animals in regard to MLC2v phosphorylation, suggesting the existence of as-yet unknown kinases in cardiac muscle cells.

Genome-wide analyses, which have recently become available in a wide range of clinical settings, such as cancer research, allow for a global view of gene expression in certain disease states and the identification of unknown molecules and molecular pathways that can be exploited as novel therapeutic targets. CHF is a candidate disease for this type of genome-wide analysis, because of its heterogeneous properties and previous difficulties identifying responsible genes using other conventional modalities.

In this study, we performed microarray analysis of the failing human myocardium and examined the correlation between the obtained genomic data and the clinical, physiological, and biochemical characteristics of CHF. In this manner, we sought to identify candidate genes that are involved in the pathophysiology of CHF. Consequently, we identified what we believe to be a novel

**Nonstandard abbreviations used:** ANP, atrial natriuretic peptide; BNP, brain natriuretic peptide; CHF, chronic heart failure; cardiac-MLCK, cardiac-specific MLCK; Dd, end-diastolic dimension; Ds, end-systolic dimension; FS, fractional shortening; hpf, hours postfertilization; MI, myocardial infarction; MLC2v, myosin regulatory light chain 2, ventricular/cardiac muscle isoform; MLCK, myosin light chain kinase; M-mode, motion mode; MO, morpholino antisense oligonucleotide; p-s15MLC, antibodies for phosphorylated MLC2v; PAP, pulmonary arterial pressure; RcMK, antibodies specific for rodent cardiac-MLCK; si-cMK, siRNA targeting cardiac-MLCK; si-smMK, siRNA targeting rat smMLCK; skMLCK, skeletal muscle MLCK; smMLCK, smooth muscle MLCK; tMLC, antibodies for total MLC2v; z-, zebrafish; z-cMKaugMO, MO targeting the AUG translational start site of  $\alpha$ -cardiac-MLCK.

**Conflict of interest:** The authors have declared that no conflict of interest exists.

**Citation for this article:** *J. Clin. Invest.* 117:2812-2824 (2007). doi:10.1172/JCI30804.